Masteroppgave

NTNU
Norges teknisk-naturvitenskapelige universitet

Veronica Galantucci

Prediction of coalescence and rebound of fluid particles in non-Newtonian media through film drainage modeling

Master’s thesis in Chemical Engineering - Joint Nordic Master's degree programme

Masteroppgave i TKP4900
Veileder: Hugo Atle Jakobsen
Medveileder: Suat Canberk Ozan
Juli 2023

NTNU
Kunnskap for en bedre verden

Veronica Galantucci

Prediction of coalescence and rebound of fluid particles in non-Newtonian media through film drainage modeling

Master’s thesis in Chemical Engineering - Joint Nordic Master's degree programme

Masteroppgave i TKP4900
Veileder: Hugo Atle Jakobsen
Medveileder: Suat Canberk Ozan
Juli 2023

Norges teknisk-naturvitenskapelige universitet

NTNU

Kunnskap for en bedre verden

Abstract

The drainage of a non-Newtonian film entrapped between two fluid particles that are moving toward one another with time-dependent velocities, causing either coalescence and rebound, is examined in this thesis. Attention is given to the non-Newtonian rheology of the continuous phase where particles disperse, in order to better understand how particles coalesce and rebound, which is important in a variety of natural processes and industrial applications. It is specifically anticipated that the non-Newtonian continuous phase will adhere to the power law model. The interfaces are permitted to deform during drainage. Non-Newtonian flows are formed when materials are processed by procedures like coating, soap solutions, or polymer extrusion.

Acknowledgement

As soon as my year of study in Bergen ended, for seven long years I dreamed of returning to Scandinavia to study. I loved everything about these places, the nature, the sport, the people I've met along the way. This double degree split between Stockholm and Trondheim will forever remain in my heart as a beautiful journey. They were two very different years, both in terms of my experiences, the way I looked at the world, and what I learned at the two different universities. First, I want to thank my peers of these two years: Carlos, Felix, Ahmed, Amalia, Aliz and Parul. Many are trips that have bonded us, as many the hours we spent at the lab and the assays we wrote, but not as many as the misadventures we had in the bad Scandinavian weather. The icy winds that constantly blow here in the north, that shake our bikes and our souls and make us shiver underneath the numerous layers of wool clothes, make us regret our distant warm countries. But despite all the bad words, the truth is only one: we have loved these places, we have loved everything about them and we will miss them dearly, just as I will miss you who have been a family during this journey. I have found many families up here in the north. Starting with my flatmates from Skyttevagen 2: Annje, Florian, and Dylan, if I ever had brothers, I would have wanted them like you. How much joy, moral support and how many laughs you have given me. Thank you for the introspective wintertime we had together and for the bold, adventurous fun during the endless summer. And with endless I refer to the sun never setting below the horizon, because summer lasts a week and then the rain comes until it is too cold even for the sky to cry. However, the family I found here in Norway did not share the same walls of the house with me, but those of the restaurant. Frati was like a mother to me, but not a mother who soothes you to sleep, but rather a mother who reprimand her daughter because she is in her adolescent and rebellious phase and the mother in question was all over me, pressing me to do things well and better, asking me to give 120% of myself, concentration and sweat, while I'm tired all the time and I aim to get the money to pay the rent and to have some fun as every expat student. And facts, there was less and less time to have fun because in addition to being a cook, I am, above all, a student! But the more time went by, the more this relationship changed, evolved, I was able to better manage my time, my stress, and every night before going to bed I cried a bit less and slept a bit more and, in the end, I'm also grateful for this crazy experience even if it did drain my serotonin levels from time to time. I don't think I am meant to be a chef, but the people I found in there will always remain in my heart, from Ilaria and Greta, to Matteo, Giuliano, Mattia, Maxi, Linda and Ale, Nicola, and mostly Nicolò, the real mama there. You are a cheerful piece of Italy that shines in Trondheim. You are so Beautiful!

With tears in my eyes, I would like to thank my friends from Italy for always supporting me in my choice to pursue my studies abroad. Thank you for always encouraging me to fly and fight for my dreams. I promise you that I will always prepare a warm bed for when you come to visit me wherever I will end up in the world. Anyway, you already know we will sleep in some sort of mountain hut or at some bizarre Italian friend's house because, mammamia, these Italians are everywhere! Thanks to le Limoncine: Cristina, Irene, Benny, Stefy, Emily and Alessia. Thanks to my fellow Sevesine, my favorite country-goose-ladies (yes, like in the Aristocats): Noemi and Martina. Girls, you all are my greatest joy. I love you immensely, to the moon and back. On one hand, my heart aches for not having shared the last years of my master's degree with you in Milan. But you know, I had this rush, this feeling that I had to come up here and that couldn't be ignored! And it was worth all the way. Thanks Andre Garg and Bus, without you I would never have figured out how to get started with MATLAB and I would never have discovered how much I love fluid dynamics. You are among the people I respect and admire the most in the world.

Finally, I would like to thank my teachers: Hugo, your explanations have always been clear and precise, your love for equations is so sincere, I admire you so much. Canberk, you are the one who had to spend the most time with me and who had to be the most patient. I learned a lot from you, you are truly an exceptional person and with a vast knowledge. Thanks for making me grow and mature this year.

Now who knows where my next adventures will take me... I will miss going Nordic skiing in Bymarka and then running to work to toast some Bruschetta Parma and spending the night in front of the computer running simulation after simulation. It is bizarre to think I will no longer be here in northern Europe... but who knows where life takes us!

List of Figures

1 Physical system . . . 4
2 curve fitting of the drag correction factor X for unbounded fluid in a power-law fluid. Data fitting from Dazhi and Gu et al. (1985) . . . 19
3 curve fitting of the drag correction factor values C_D for spheres in dilatant fluids. Curves are fitted for different n values: 1 (Newtonian case), 1.2, and 1.4. Raw data from: Tripathi et al. (2006) . . . 21
4 curve fitting of the $f(Re)$ from the C_D values for spheres in dilatant fluids. Curves are fitted for different n values: 1 (Newtonian case), 1.2, and 1.4. Raw data from: Tripathi et al. (2006) . . . 21
5 Evolution of $V_{app0,guess}$ with search iterations until convergence to V_c along the iteration steps. . 24
6 Pressure and Film Thickness. The model parameters are: $V_{app} = 0.05$, $A^* = 0.0001$, time steps $dt = 0.01$. The simulation result is marked by circles and the black curve shows the reference from Fanebust et al. (2021) . . . 25
7 Effect of particle radius on V_c in a Newtonian system. The simulation result is marked by circles and the black curve shows a fit based on the reference adapted from Ozan et al. (2023) . . . 26
8 A collision with rebound outcome: (a) film thickness profiles, (b) minimum film thickness, (c) the approach velocity, and (d) the total film force acting on the particles as functions of time. The model parameters are $Rp = 0.001$, $V_{app,0} = 1 \times 10^{-4}$, $V_{2,0} = -V_{1,0} = V_{app,0}/2$, $h_{min,0} = 0.1$, $Oh_A^2 = 8.2 \times 10^{-6}$, $A^* = 10^{-13}$ and $n = 0.95$. . . . 27
9 Non-physical coalescence outcome. Film thickness profiles during particles approach. The model parameters are $Rp = 0.001$, $V_{app,0} = 1 \times 10^{-4}$, $V_{2,0} = -V_{1,0} = V_{app,0}/2$, $h_{min,0} = 0.1$, $Oh_A^2 = 8.2 \times 10^{-6}$, $A^* = 10^{-13}$ and $n = 0.95$. . . . 28
10 A collision with steady-state outcome: (a) film thickness profiles, (b) minimum film thickness, (c) the approach velocity, and (d) the total film force acting on the particles as functions of time. The model parameters are $Rp = 0.001$, $V_{app,0} = 1 \times 10^{-4}$, $V_{2,0} = -V_{1,0} = V_{app,0}/2$, $h_{min,0} = 0.1$, $Oh_A^2 = 8.2 \times 10^{-6}$, $A^* = 10^{-13}$ and $n = 0.95$. . . . 29
11 Comparison of the h_{min} for Newtonian and power law drag force expressions at the same approach velocity $V_{app} = 0.0003$, and $Rp = 0.0005$. . . . 30
12 Comparison of the effect of the Newtonian and the non-Newtonian drag force expressions of an unbounded fluid in a power-law fluid on the critical velocity . . . 30
13 Time evolution of the minimum film thickness for different n: initial approach velocity $V_{app0} = 0.0003$ and $Rp = 0.0005$. Most of the cases at this initial approach velocity show steady-state outcome. On the left, three cases, for $n < 1$, show coalescence. The plot on the left is on logarithmic scale for the $y-$axis. . . . 31
14 Time evolution of the film thickness for shear-thinning fluids ($n < 1$) and shear-thickening fluids ($n > 1$), $Rp = 0.001$ . . . 31
15 Effect of the power-law index on the critical velocity for different type of fluids. . . . 32
16 Effect of different flow consistency index on the critical velocity plot. The model parameters are V_cs from the simulation for Rp=0.0008 and n=0.95, $\sigma = 0.0728$ . . . 33
17 Plot of the h_{min} at the rebound of particles for $n = 0.70$ and $R_p = 0.0005$ . . . 33

Contents

1 Introduction **1**
- 1.1 Coalescence . . . 1
- 1.2 Film Drainage . . . 1
- 1.3 Rheology . . . 2
- 1.4 Dispersed systems . . . 3
- 1.5 Sustainable goal . . . 4

2 Mathematical Model **4**
- 2.1 Newtonian Model . . . 5
  - 2.1.1 Governing equations . . . 5
  - 2.1.2 Interface conditions . . . 7
  - 2.1.3 Non-Dimensionalization . . . 9
  - 2.1.4 Analytical solution of the model . . . 11
- 2.2 Power Law . . . 13
  - 2.2.1 Dimensionless Equations . . . 13
  - 2.2.2 Dimensionless Power law . . . 13
  - 2.2.3 Analytical solution with Power law . . . 15
- 2.3 Force Balance . . . 17
  - 2.3.1 Critical Rebound Velocity . . . 18
- 2.4 Power-law drag effect on a particle . . . 19
  - 2.4.1 Shear-thinning fluids . . . 19
  - 2.4.2 Shear-thickening fluids . . . 20

3 Numerical Procedure **22**
- 3.1 Newtonian solver . . . 22
- 3.2 Non-Newtonian case solver . . . 24
- 3.3 Implementation of force balance and search algorithm . . . 24

4 Results and Discussion **25**
- 4.1 Validation . . . 25
  - 4.1.1 Validation of the Non-newtonian code . . . 25
  - 4.1.2 Validation of the Force balance . . . 25
- 4.2 Rebound and Coalescence . . . 26
- 4.3 Force Balance . . . 28
  - 4.3.1 Newtonian continuous media vs Power law type drag force . . . 28
- 4.4 Effects of Power law parameters . . . 28
  - 4.4.1 Effect of the flow behavior index, n . . . 28
  - 4.4.2 Effect of the flow consistency index, k . . . 32
  - 4.4.3 Challenges and future work . . . 33

5 Conclusions **35**

A MATLAB code **37**
- A.1 Non-Newtonian Solver . . . 37
- A.2 Force Balance . . . 40

1 Introduction

Multi-phase systems in which the dispersed fluid particles interact with each other and with the continuous phase are ubiquitous phenomena in everyday life. From a technological standpoint, numerous operations in chemical engineering and processing industries involve fluid-particle systems. The term 'fluid particles' covers here both droplets and bubbles since multi-phase frameworks frequently feature interaction of liquid metals, a gas (commonly air) top space, liquid droplets in the top space, and injection of both solid particles and gaseous bubbles into the bath. Monitoring and modeling the behavior of such interactions play a crucial role in many chemical industries. Additionally, in many of these processes, it is not rare that the continuous phase is a non-Newtonian substance, such as polymeric melts and solutions, crude oil, or biofuels. These fluids do not have a linear relationship between shear stress and shear rate, unlike the widely studied and described Newtonian fluids. In other words, the viscosity of a non-Newtonian fluid is a function of the shear rate, rather than being constant as it is for the Newtonian ones (Peng at al, 2014). On the contrary to the general understanding, they are much more common than Newtonian fluids in nature. Therefore, it is extremely important to analyze the effect of the viscosity of such fluids and reveal the impact of the rheological complexities on the flow characteristics, which can alter the efficiency and performance of the reactor considerably.

1.1 Coalescence

Coalescence is an energy minimization phenomenon in which two drops or bubbles merge to form a thermodynamically stable daughter particle. Coalescence of particles of Newtonian fluids plays a key role in rain drop condensation, combustion, atomization of metal droplets; while non-Newtonian fluid particles coalescence finds applications in food industry, spray coating and paintings, even processes linked to life like those in growth and development of tumor.

Any multiphase process involves several interactions, some of which may result in droplet and particle collisions. In all processes involving phase separation that require destabilizing emulsions during treatment or purification procedures, such as natural gas production, where the breakdown and separation of foams, water-in-oil or oil-in-water emulsions is essential for process effectiveness, coalescence plays a significant role. Bubble coalescence significantly influences the operation's performance depending on the process, particularly when little air bubbles are carried away in low shear stress zones or when the fine distribution of one phase into another is necessary (Dudek et al., 2020).

In dispersed flow modeling, which frequently uses the population balance framework, the influence of coalescence and breakage is accounted for by source and sink terms, which stand for the creation of a new fluid particle and the demise of the previous ones, respectively. These source/sink concepts use an equation for the coalescence frequency. The collision frequency, or how frequently the fluid particles collide within the dispersed flow, and the coalescence probability of the interacting fluid particles are typically multiplied to indicate the coalescence frequency.

For the coalescence process, three ideas or criteria have often been put forth. The film drainage model is the most widely accepted theory. According to Shinnar and Church (1960), two bubbles may cohere together after colliding and be prevented from coalescing by a thin layer of liquid caught between them. However, Howarth (1964) asserts that the coalescence probability is controlled by the turbulent force and not by the attraction between two colliding interfaces, and that the coalescence probability depends on the impact of colliding bubbles. When "energetic collisions" occur, which occur when the approach velocities of two colliding bubbles exceed a certain value, instantaneous coalescence without the formation of a liquid film rim and thinning of it will be the predominant process. The critical approach velocity model, which is an empirical theory based on the experimental finding of Doubliez (1991) and Duineveld (1994) that tiny approach velocities result in a high coalescence efficiency, was presented in more recent research, as demonstrated by Liao and Lucas (2010).

Coalescence is not always the result of collision. There are several ways to explain when a collision causes coalescence and when it doesn't. The liquid layer between the particles must drain to the critical size essential to break it before coalescence may occur. This contact between the particles must last for a sufficient amount of time. In other words, the rate of film thinning determines whether coalescence will occur.

1.2 Film Drainage

The film drainage model, which identifies three distinct stages of the process—collision, film drainage, and film rupture—is the most popular one for describing coalescence. A drop may collide with another by agitation, gravity, or Brownian motion. When two particles are approaching, a thin film of the continuous phase forms between them. The film needs to be drained to a critical thickness where strong attractive forces cause the film to break down and allow the two particles to coalesce into one. In this method, the coalescence probability is calculated by comparing the coalescence time scale to the interaction time scale. Hydrodynamic modeling of the drainage of the thin layer between two approaching fluid particles prior to coalescence is frequently used to

determine the coalescence time. This method is based on observations made by Shinnar and Church (1960), who identified three steps in the coalescence process: first, the particles start interacting as they come closer to one another and entrap a thin film of the continuous phase. Once the liquid layer between the two bubbles has drained to a crucial thickness indicative of coalescence, it finally raptures as a result of the approaching motion. The particles are often assumed to collide "gently" in the film drainage modeling, i.e., the radius of the entrapped thin film is much smaller than the particle radii.

The constant approach velocity is found to affect coalescence in three different ways. Three successive film drainage regimes were found by Ozan and Jakobsen (2019a) at different approach velocities. Lower approach velocities cause the film rupture to happen at the film's center, and higher approach velocities cause the coalescence period to shorten. The dimple development is seen when the approach velocity rises, and the film tears at the rim. When operating in this second regime, the coalescence time gets shorter as the approach velocity gets faster until it achieves a minimum. Following this minimum, the third stage is reached, where secondary rim structures start to develop at the interface and the coalescence time starts to lengthen as the approach velocity increases.

The lubrication theory is used to simplify the hydrodynamic models since the film between the particles is thin. Additionally, a key factor in creating more precise film drainage models is how the interface is handled. There are various levels of intricacy involved here. To start, because the interface thicknesses are so much less than the film thickness, the three-dimensional particle interfaces can be viewed as two-dimensional surfaces. In this 2-dimension model, where the interfaces have no mobility the tangential interface velocity is zero but the interfaces are still allowed to deform. The simplest scenario is non-deformable spherical particles with immobile interfaces, i.e., with zero tangential velocity, which allows the drainage model to be solved analytically. The simplification of no tangential mobility is plausible since immobile systems are more common due to the presence of surfactants or due to impurity effects in the system that lock the tangential motion of the interfaces as it is shown in the study of Ozan and Jakobsen (2019b). However, with a non-deformable interface it is not possible to render the dimpling of the interface, which is well-documented in experiments Derjaguin and Kussakov (1939) and known to affect the coalescence behavior significantly (Ozan et al., 2021). Therefore, allowing the interfaces to deform in the film drainage model is essential for the accuracy of the model. When the interface is immobile, the film flow is only driven by pressure gradients, producing a parabolic velocity profile; however, when the tangential velocity completely dominates the film drainage, the velocity profile appears as a plug-flow profile, and the mobility of the interface controls the film drainage (Lee and Hodgson, 1968). Regardless of the deformability of the interface, its tangential mobility determines the type of the film flow (Lee and Hodgson, 1968). The partially mobile interfaces, which take into account both the parabolic and the plug flow, are a more universal alternative to the totally mobile and immobile interfaces. In addition, high dispersed phase viscosity and Marangoni fluxes along the interface are typically related to the immobilization of the interface (Lee and Hodgson, 1968). The presence of surfactants in many real systems makes it highly likely that particle surfaces will be immobilized, especially in polymeric systems where particle and medium interaction will be improved. Surfactants in emulsions adhere to the interface and affect stability, immobilizing the interface also by increasing its viscosity, as demonstrated by Ozan and Jakobsen (2019b) and Ozan and Jakobsen (2020).

The connection of the dispersed and continuous phase velocity fields is necessary to determine the tangential velocity of the interfaces. The boundary integral technique (Davis et al., 1989) demonstrated that this linkage can be achieved through the no-slip condition and the stress balances without necessitating the solution of the particles' internal flow. The cost of computation is significantly reduced as a result. The usage of this approach is well documented in the literature.

This study will be dedicated to coalescence in non-Newtonian continuous media with further examination of other parameters such as the time-dependent approach velocity, for which a force balance will be implemented. Furthermore, different closure models for the drag force will be examined. The film drainage behavior will be investigated by employing a hydrodynamic film drainage model. During the drainage, the interfaces are immobile and ideal, meaning that only the surface tension is significant to take into account. In addition, the non-Newtonian film is described by the Power Law model.

1.3 Rheology

Ever since the discovery of the laws of motion by Newton, it has been a common practice to accept the Newtonian fluid model as a standard fluid behavior, although this model can't explain experiments' outcomes and predict the behavior of the majority of fluids and especially complex multiphase systems. Despite the varied and versatile application of non-Newtonian fluids, coalescence dynamics of such fluids remain a sparsely studied area. The vastness of the domain of non-Newtonian fluids - they can range from macromolecular fluids to various colloids - makes a unified understanding even more elusive. Each subclass has a different microstructure composition leading to distinct behaviors. The branch of physics that studies the deformation and the flow of matter, establishing constitutive relations between stimuli applied on a material and the materials' responses to stimuli, is called rheology. Non-Newtonian fluids are fluids whose properties are not described

by a single constant value of viscosity. These fluids are most frequently identified by a nonlinear stress–strain relationship, yield stress, or time–dependent viscosity. Rheological complexity entails, in turn, solving nonlinear mathematical problems that haven't reached the same respectable level of progress and maturity that Newtonian fluid witnessed through the years.

The non-Newtonian fluid behavior is much more widespread than it is generally perceived. Polymer processing, pharmaceutical products, thickening agents in food processing, drag reduction applications exhibit complex rheological behaviors. Thus, over the years, due to the ever increasing needs and demands of consumers coupled with the advancements in technology, chemical and process engineering applications extensively use a wide range of rheologically complex materials including polymeric melts and solutions, and multiphase mixtures (foams emulsions, dispersions).

Rheology concerns all types of materials, but it is interesting to bind the field within two extremes: viscous fluids and elastic solids. The non-Newtonian continuous phase in this work is assumed to have no elastic properties, i.e., it is a generalized Newtonian fluid. Therefore, the focus will be on the viscous models throughout this section. Newtonian fluids are identified by a linear behavior between the shear rate and the shear strain; for those, viscosity is constant and independent of the shear rate. They follow Newton's law of viscosity:

$$\tau = -\eta\dot{\gamma} \tag{1}$$

where τ is the viscous stress, η is the viscosity, and $\dot{\gamma}$ the shear rate. Newtonian liquids are often instances of glycerine, water, and various mineral oils. The Newtonian behavior is further distinguished by constant viscosity with respect to the time of shearing and a quick relaxation of the shear tension following the cessation of shearing. Additionally, the viscosities that are measured in various forms of deformation are always in relation to one another. Generalized Newtonian fluids are substances like dispersions, emulsions, and polymer solutions that frequently deviate from the Newtonian behavior. Those show no elastic behavior and their viscosity is found to decrease or increase with increasing shear rate, referring to shear thinning and shear thickening respectively. The most common model used for shear-thinning and shear-thickening fluids is the power-law model:

$$\eta(\dot{\gamma}) = k\,|\dot{\gamma}|^{n-1} \tag{2}$$

where $\dot{\gamma}$ is the magnitude of $\dot{\gamma}$, k is the flow consistency index, and n the power index. This expression represents shear-thickening behavior for $n > 1$, shear-thinning behavior for $n < 1$, and Newtonian behavior for $n = 1$. Shear-thickening behavior is much less frequent but might occur in some dispersions and specific suspensions with a high solid particle concentration. Shear-thinning behavior is the most frequent form of non-Newtonian behavior in industrial applications. Shear-thickening is often an undesirable consequence that can seriously affect processing. The non-Newtonian viscosity may be calculated most easily, and it does so well for modest shear rates, using the power law model. For low and high shear rates, the viscosity becomes almost constant, however, and the power law model is unable to produce reliable findings. The Sisko model, for example, would be a better option to estimate the viscosity because it applies for shear rates in the power law area in addition to higher shear rates. The Sisko model is defined as (Barnes 2000):

$$\eta(\dot{\gamma}) = k\,|\dot{\gamma}|^{1-n} + \eta_\infty\,|\dot{\gamma}| \tag{3}$$

where η_∞ is the viscosity value at high shear rate. For the entire range of shear rates, the Cross model (Barnes 2000),

$$\frac{\eta(\dot{\gamma}) - \eta_\infty}{\eta_0 - \eta_\infty} = \frac{1}{1 + k\,|\dot{\gamma}|^n} \tag{4}$$

can be employed. Here, η_0 is the viscosity at a low shear rate. However, in this thesis, the shear rates are assumed to be within the range describable by the power law.

1.4 Dispersed systems

Multiphase dispersed systems are systems that deal with at least two immiscible phases in contact; therefore, the understanding of physical and chemical phenomena that occur at interfaces or at the layers close to the interfaces, is of substantial interest. The design of suitable chemical reactors, as well as their subsequent downstream processing, storage, and transportation, are all influenced by the stability of two-phase dispersions systems, making it essential to model the impacts of these numerous elements. For instance, an emulsion is a dispersion system that permits the creation of particles as a result of shear stress and the tension at the fluid-liquid interface. To create efficient emulsion systems, it is essential to optimize the flow rate, solution viscosity, and surface tension. Another example in the industry could be the supply of oxygen for aerobic fermentations in a yeast fermentor. The more the system is dispersed, the more microbubbles of air are inside, the higher the mass transfer, the more are the reactants converted into the fermentation products. For such systems, it is of crucial importance to have a highly dispersed system for a higher surface area. Furthermore, it is crucial to characterize the microstructure and flow characteristics of dispersions in order to comprehend, regulate, and guarantee their optimal performance.

1.5 Sustainable goal

According to Hasanbeigi (2018) in the journal "Energy Efficiency in California's Chemical Industry," the chemical sector, which includes petrochemicals, is one of the leading emitters of greenhouse gases (GHG), accounting for around 20% of global GHG emissions. Energy is a major resource for our civilization today and will be essential for our sustainability in the future, thus reducing CO2 emissions and maximizing process efficiency are essential. Efficiency's greatest adversary is friction, which requires a significant amount of energy to overcome, particularly in the transportation, industrial, and power-generation sectors. The effectiveness of lubricating oil may be greatly increased by modern technologies. The viscosity of a lubricating oil has a significant impact on how effectively it reduces friction and wear. The majority of lubricants now produced employ mineral oils as their base constituents, which are created by refining petroleum oils. Mineral oils are replaced with synthetic oils, which are made of chemical compounds. Chemical additives are typically added to lubricants to increase oil life, prevent corrosion, minimize friction and wear, lower temperature and its effects, and lessen sludge buildup in engines. Typically, these oils are categorized as non-Newtonian.

Even if the bulk of lubricant components now used are made from fossil carbon sources, a significant amount of material is still present due to the size of the entire market for these products. According to Boyde (2002), lubricants made from renewable raw materials are thought to make up around 2% of the market in Europe.

2 Mathematical Model

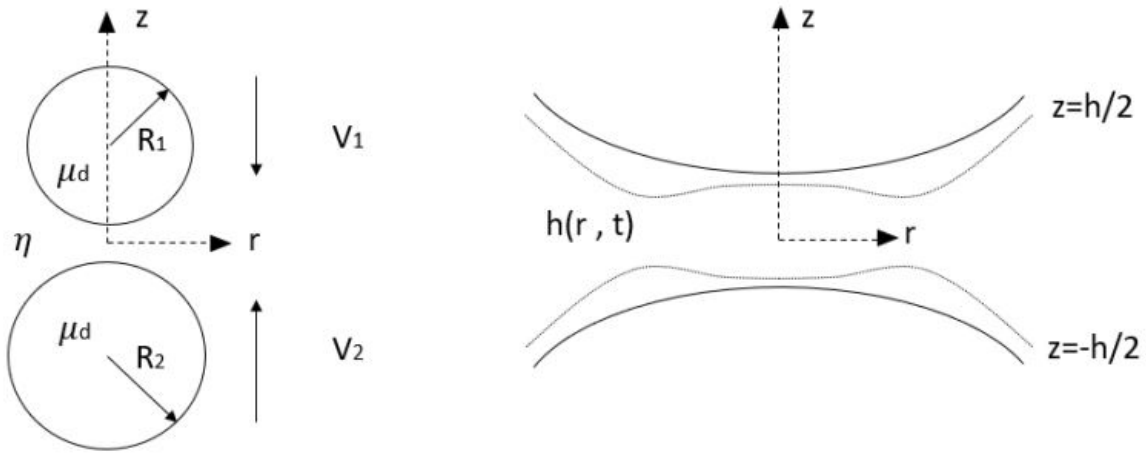

Figure 1: Physical system

To obtain the theoretical solution for the film drainage model, the symmetry of the problem is employed and equations are formulated in two-dimensional Cartesian coordinates. Figure 1 illustrates the physical configuration of two particles that are allowed to have different radii,R_1 and R_2, and are approaching each other along their centerline with velocities $V_1(t)$ and $V_2(t)$ and a thin film of the non-Newtonian continuous phase is entrapped between them and assumed to be incompressible. The continuous phase has viscosity η, following the Power law. Meanwhile, the dispersed phase is assumed incompressible Newtonian fluid, characterized by constant viscosity μ_d. Interfaces are assumed deformable and assumed to be inviscid and its rheological behavior is described by the surface tension, σ, assumed constant. The axisymmetrical interactions between two fluid particles in non-Newtonian continuous media are examined. Since, for assumptions, the particles are assumed to collide gently, the particles' radii are much larger than the radius of the entrapped film. As a result, both particles can be described by the equivalent radius, R_p (Abid and Chesters 1994):

$$\frac{1}{R_p} = \frac{1}{2}\left(\frac{1}{R_1} + \frac{1}{R_2}\right) \tag{5}$$

The collision between the particles can now be modeled as a collision of particles of equal size with radius R_p. For these reasons, the system is assumed symmetric around the radial axis in addition to axisymmetric. This simplifies the geometry of the problem and the solutions can be obtained just for a quadrant of the film, where $r \geq 0$and $z \geq 0$, and the interface position is given by $z = h/2$. In Fig. 1, the classical dimple formation is shown which is possible only when drainage occurs for deformable interfaces. Such model implies numerical simulations.

The thin film has thickness $h(r,t)$, which is a function of the radial position r and the time t. This thin film has a thickness typically much smaller than its radial extent, rendering the lubrication theory applicable. First, the drainage model will be derived for a Newtonian continuous phase in Chapter 2.1.1. Then, the model will be expanded for a non-Newtonian fluid with a non-constant viscosity and the Power law model will be introduced in Chapter 2.2.

Furthermore, the governing and interface equation will be rendered dimensionless together with the viscosity model and containing the Hamaker constant for the pressure equation. The Hamaker constant is a coefficient that relates the interactive Van Der Waals energy to the distance of separation between two molecules, used to evaluate the interaction between molecules based on composition and structure of the particle, as widely used from previous studies (Abid and Chesters, 1994).

Only after displacing all the main equation to solve the problem, the time-dependent behavior of the approach velocity will be modeled by a force balance in Chapter 2.3.

2.1 Newtonian Model

2.1.1 Governing equations

Governing equations are universally valid equations derived from the bulk phase. In particular, the equations used are mass and momentum conservation. The continuity equation is defined by:

$$\frac{\partial \rho}{\partial t} + \nabla \cdot (\rho \mathbf{v}) = 0 \tag{6}$$

where ρ is the density of the continuous phase, t the time and $\mathbf{v}$ is the continuous phase velocity vector. The continuity equation may be expressed as follows if we assume an incompressible flow:

$$\nabla \cdot (\mathbf{v}) = 0 \tag{7}$$

The equation can be further simplified by applying the assumption of axisymmetry, which implies that the velocity along the θ-direction is constant, and applying the definition of the nabla operator and decomposing the velocity in cylindrical coordinates the following is found:

$$\left(\mathbf{e}_r \frac{\partial}{\partial r} + \frac{1}{r}\mathbf{e}_\theta \frac{\partial}{\partial \theta} + \mathbf{e}_z \frac{\partial}{\partial z}\right) \cdot (v_r \mathbf{e}_r + v_z \mathbf{e}_z) = 0 \tag{8}$$

in this work $v_\theta = 0$ is assumed. Derivatives are simplified using the product rule of derivatives. Unlike the cartesian nabla operator, derivatives of unit vectors are not equal to zero neither are kept out of the derivation as constants. This is because cylindrical unit vectors are not universally constant. Though their magnitude is equal to 1, they can still have different directions. Then knowing this, after applying the dot product the equation results in:

$$\nabla \cdot (\mathbf{v}) = \frac{\partial v_r}{\partial r} + \frac{v_r}{r} + \frac{\partial v_z}{\partial z} \tag{9}$$

By writing the first two-term for consistency, the continuity equation becomes:

$$\frac{1}{r}\frac{\partial}{\partial r}(r v_r) + \frac{\partial v_z}{\partial z} = 0 \tag{10}$$

The equation of motion is defined by:

$$\frac{\partial}{\partial t}(\rho \mathbf{v}) + \nabla \cdot (\rho \mathbf{v}\mathbf{v}) = -\nabla P - \nabla \cdot \tau + \rho \mathbf{g} \tag{11}$$

where the gravitational accelerator vector is $\mathbf{g}$, P represents pressure, and τ is the viscous stress tensor. The same incompressible flow assumption may be used, making ρ constant and changing the first term in the formula to:

$$\frac{\partial}{\partial t}(\rho \mathbf{v}) = \rho \frac{\partial}{\partial t}(v_r e_r + v_z e_z) \tag{12}$$

The second component in the equation of motion is changed to the following by applying the nabla vector definition and the dyadic velocity product:

$$\nabla \cdot (\rho \mathbf{v}\mathbf{v}) = \left(\mathbf{e}_r \frac{\partial}{\partial r} + \frac{1}{r}\mathbf{e}_\theta \frac{\partial}{\partial \theta} + \mathbf{e}_z \frac{\partial}{\partial z}\right) \cdot \rho \left(v_r v_r \mathbf{e}_r \mathbf{e}_r + v_r v_z \mathbf{e}_r \mathbf{e}_z + v_z v_r \mathbf{e}_z \mathbf{e}_r + v_z v_z \mathbf{e}_z \mathbf{e}_z\right) \tag{13}$$

By using the dot product between cylindrical unit base vectors and the definition of unit base vector derivatives, Eq. 13 can be reformulated as:

$$\nabla \cdot (\rho \mathbf{v}\mathbf{v}) = \rho \left[\frac{\partial}{\partial r}(v_r v_r \mathbf{e}_r) + \frac{\partial}{\partial r}(v_r v_z \mathbf{e}_z) + \frac{v_r v_r}{r}\mathbf{e}_r + \frac{v_r v_z}{r}\mathbf{e}_z + \frac{\partial}{\partial z}(v_z v_r \mathbf{e}_r) + \frac{\partial}{\partial z}(v_z v_z \mathbf{e}_z)\right] \tag{14}$$

Utilizing the product rule and the definition of unit base vectors derivatives, Eq. 14 can be expressed as:

$$\nabla \cdot (\rho \mathbf{v}\mathbf{v}) = \rho \left[\mathbf{e}_r \frac{\partial}{\partial r} (v_r v_r) + \mathbf{e}_z \frac{\partial}{\partial r} (v_r v_z) + \mathbf{e}_r \frac{v_r v_r}{r} + \mathbf{e}_z \frac{v_r v_z}{r} + \mathbf{e}_r \frac{\partial}{\partial z} (v_z v_r) + \mathbf{e}_z \frac{\partial}{\partial z} (v_z v_z) \right] \tag{15}$$

The third term can be expressed as:

$$-\nabla P = -\mathbf{e}_r \frac{\partial P}{\partial r} - \mathbf{e}_z \frac{\partial P}{\partial z} \tag{16}$$

The assumption of axisymmetric flow is still employed resulting in no angular pressure gradient term. By using this assumption, the fourth term can be rewritten as:

$$\nabla \cdot \tau = \left(\mathbf{e}_r \frac{\partial}{\partial r} + \frac{1}{r} \mathbf{e}_\theta \frac{\partial}{\partial \theta} + \mathbf{e}_z \frac{\partial}{\partial z} \right) \cdot (\tau_{rr} \mathbf{e}_r \mathbf{e}_r + \tau_{rz} \mathbf{e}_r \mathbf{e}_z + \tau_{\theta\theta} \mathbf{e}_\theta \mathbf{e}_\theta + \tau_{zr} \mathbf{e}_z \mathbf{e}_r + \tau_{zz} \mathbf{e}_z \mathbf{e}_z) \tag{17}$$

The angular derivatives of all the scalars are zero due to axisymmetry. By performing the dot product, applying the product rule and the unit base vector derivatives, the divergence of the stress tensor can be rearranged to:

$$\nabla \cdot \tau = \frac{\partial}{\partial r} (\tau_{rr} \mathbf{e}_r) + \frac{\partial}{\partial r} (\tau_{rz} \mathbf{e}_z) + \frac{\tau_{rr}}{r} \mathbf{e}_r - \frac{\tau_{\theta\theta}}{r} \mathbf{e}_r + \frac{\partial}{\partial z} (\tau_{zr} \mathbf{e}_r) + \frac{\partial}{\partial z} (\tau_{zz} \mathbf{e}_z) \tag{18}$$

Equation 18 is manipulated further by use of the product rule obtaining:

$$\nabla \cdot \tau = \mathbf{e}_r \frac{\partial}{\partial r} (\tau_{rr}) + \mathbf{e}_z \frac{\partial}{\partial r} (\tau_{rz}) + \mathbf{e}_r \frac{\tau_{rr}}{r} - \mathbf{e}_r \frac{\tau_{\theta\theta}}{r} + \mathbf{e}_r \frac{\partial}{\partial z} (\tau_{zr}) + \mathbf{e}_z \frac{\partial}{\partial z} (\tau_{zz}) \tag{19}$$

It is presumed that the last term in the equation of motion is negligible in comparison to the other components.

The equation of motion then has the following form:

$$\begin{aligned} &\rho \left[\frac{\partial}{\partial t} (v_r e_r + v_z e_z) + \mathbf{e}_r \frac{\partial}{\partial r} (v_r v_r) + \mathbf{e}_z \frac{\partial}{\partial r} (v_r v_z) + \mathbf{e}_r \frac{v_r v_r}{r} + \right. \\ &\left. \mathbf{e}_z \frac{v_r v_z}{r} + \mathbf{e}_r \frac{\partial}{\partial z} (v_z v_r) + \mathbf{e}_z \frac{\partial}{\partial z} (v_z v_z) \right] = -\mathbf{e}_r \frac{\partial P}{\partial r} - \mathbf{e}_z \frac{\partial P}{\partial z} - \mathbf{e}_r \frac{\partial}{\partial r} (\tau_{rr}) \\ &- \mathbf{e}_z \frac{\partial}{\partial r} (\tau_{rz}) - \mathbf{e}_r \frac{\tau_{rr}}{r} + \mathbf{e}_r \frac{\tau_{\theta\theta}}{r} - \mathbf{e}_r \frac{\partial}{\partial z} (\tau_{zr}) - \mathbf{e}_z \frac{\partial}{\partial z} (\tau_{zz}) \end{aligned} \tag{20}$$

By decomposing the equation of motion, the r-component becomes:

$$\rho \left[\frac{\partial v_r}{\partial t} + \frac{\partial}{\partial r} (v_r v_r) + \frac{v_r v_r}{r} + \frac{\partial}{\partial z} (v_z v_r) \right] = -\frac{\partial P}{\partial r} - \frac{\partial \tau_{rr}}{\partial r} - \frac{\partial \tau_{rr}}{\partial r} - \frac{\tau_{rr}}{r} + \frac{\tau_{\theta\theta}}{r} - \frac{\partial \tau_{zr}}{\partial z} \tag{21}$$

By applying the product rule, the terms containing the partial derivative of v_r can be rewritten as:

$$\rho \left[\frac{\partial v_r}{\partial t} + \frac{1}{r} \frac{\partial}{\partial r} (r v_r v_r) + \frac{\partial}{\partial z} (v_z v_r) \right] = -\frac{\partial P}{\partial r} - \frac{1}{r} \frac{\partial}{\partial r} (r \tau_{rr}) - \frac{\tau_{rr}}{r} + \frac{\tau_{\theta\theta}}{r} - \frac{\partial \tau_{zr}}{\partial z} \tag{22}$$

whereas, the z-component yields:

$$\rho \left[\frac{\partial v_z}{\partial t} + \frac{\partial}{\partial r} (v_r v_z) + \frac{v_r v_z}{r} + \frac{\partial}{\partial z} (v_z v_z) \right] = -\frac{\partial P}{\partial z} - \frac{\partial \tau_{rz}}{\partial r} - \frac{\partial \tau_{zz}}{\partial z} \tag{23}$$

Again, by applying the product rule, the terms containing the partial derivative of v_r can be rewritten as:

$$\rho \left[\frac{\partial v_z}{\partial t} + \frac{1}{r} \frac{\partial}{\partial r} (v_r v_z) + \frac{\partial}{\partial z} (v_z v_z) \right] = -\frac{\partial P}{\partial z} - \frac{\partial \tau_{rz}}{\partial r} - \frac{\partial \tau_{zz}}{\partial z} \tag{24}$$

Newton's law may be used to construct the viscous stress tensor for Newtonian fluids as:

$$\tau_{rr} = -2\mu \frac{\partial v_r}{\partial r} \tag{25}$$

$$\tau_{rz} = \tau_{zr} = -\mu \left(\frac{\partial v_z}{\partial r} + \frac{\partial v_r}{\partial z} \right) \tag{26}$$

$$\tau_{\theta\theta} = -2\mu \frac{v_r}{r} \tag{27}$$

$$\tau_{zz} = -2\mu \frac{\partial v_z}{\partial z} \tag{28}$$

where μ is the Newtonian continuous phase viscosity. The final formulations for the r- and z-components of the equation of motion are as follows after incorporating these equations into Eqs. 22 and 24:

$$\begin{aligned}\rho\left[\frac{\partial v_r}{\partial t}+\frac{1}{r}\frac{\partial}{\partial r}\left(rv_rv_r\right)+\frac{\partial}{\partial z}\left(v_zv_r\right)\right]=\\ -\frac{\partial P}{\partial r}+\frac{1}{r}\frac{\partial}{\partial r}\left(2\mu r\frac{\partial v_r}{\partial r}\right)-2\mu\frac{v_r}{r}-\frac{\partial}{\partial z}\left[-\mu\left(\frac{\partial v_z}{\partial r}+\frac{\partial v_r}{\partial z}\right)\right]\end{aligned} \tag{29}$$

$$\rho\left[\frac{\partial v_z}{\partial t}+\frac{1}{r}\frac{\partial}{\partial r}\left(v_rv_z\right)+\frac{\partial}{\partial z}\left(v_zv_z\right)\right]=-\frac{\partial P}{\partial z}+\frac{\partial}{\partial r}\left[\mu\left(\frac{\partial v_z}{\partial r}+\frac{\partial v_r}{\partial z}\right)\right]-\frac{\partial}{\partial z}\left(-2\mu\frac{\partial v_z}{\partial z}\right) \tag{30}$$

2.1.2 Interface conditions

The interface conditions are additional equations employed only as a boundary condition valid on the interface but also related to the variables of the bulk phases. These equations include the kinematic condition, the no-slip condition, and the normal and tangential stress balance components. With a set of boundary conditions that are only true at the interface, those equations link the continuous and dispersed phase variables. The unit tangent and the normal vectors on the interface must first be defined. As the solution will be only recovered for $r \geq 0$ and $z \geq 0$, the interface position is given by:

$$z=\frac{1}{2}h\left(r,t\right)=f \tag{31}$$

where f is a function that represents the surface. The normal vector $\mathbf{n}$ is defined by:

$$\mathbf{n}=\mathbf{n}\left(r,t\right)=-\frac{\nabla f}{|\nabla f|} \tag{32}$$

Since ∇f is defined by:

$$\begin{aligned}\nabla f&=\mathbf{e}_r\frac{\partial f}{\partial r}+\mathbf{e}_\theta\frac{\partial f}{\partial \theta}+\mathbf{e}_z\frac{\partial f}{\partial z}\\ &=-\frac{1}{2}\frac{\partial h}{\partial r}\mathbf{e}_r+\mathbf{e}_z\end{aligned} \tag{33}$$

where the angular term disappears due to axisymmetry. The normal vector then can be written as:

$$\mathbf{n}=\frac{-\frac{1}{2}\frac{\partial h}{\partial r}\mathbf{e}_r+\mathbf{e}_z}{\sqrt{1+\frac{1}{4}\left(\frac{\partial h}{\partial r}\right)^2}} \tag{34}$$

There are two tangent vectors in the system: one is $\mathbf{e}_\theta$, which requires no further manipulation, and the other is defined as:

$$\mathbf{t}=\mathbf{t}\left(r,t\right)=\frac{\frac{\partial \mathbf{r_s}}{\partial r}}{\left|\frac{\partial \mathbf{r_s}}{\partial r}\right|} \tag{35}$$

which depends on both time t and position r. In cylindrical coordinates, the position vector $\mathbf{r}$ is represented as follows:

$$\mathbf{r}=r\mathbf{e}_r+z\mathbf{e}_z \tag{36}$$

which, following Eq. 31, in surface coordinates becomes:

$$\mathbf{r_s}=r\mathbf{e}_r+\frac{1}{2}h\left(r,t\right)\mathbf{e}_z \tag{37}$$

The surface position vector's derivative with regard to r is as follows:

$$\frac{\partial \mathbf{r_s}}{\partial r}=\mathbf{e}_r+\frac{1}{r}\frac{\partial h}{\partial r}\mathbf{e}_z \tag{38}$$

The length of the vector is calculated as:

$$\left|\frac{\partial \mathbf{r_s}}{\partial r}\right|=\sqrt{1+\frac{1}{4}\left(\frac{\partial h}{\partial r}\right)^2} \tag{39}$$

The tangential vector $\mathbf{t}$ can then be express as:

$$\mathbf{t}=\frac{\mathbf{e}_r+\frac{1}{r}\frac{\partial h}{\partial r}\mathbf{e}_z}{\sqrt{1+\frac{1}{4}\left(\frac{\partial h}{\partial r}\right)^2}} \tag{40}$$

The interface conditions can now be derived. The no-slip condition is defined by:

$$\mathbf{v}_c \cdot \mathbf{t} = \mathbf{v}_d \cdot \mathbf{t} = \mathbf{U} \cdot \mathbf{t} \tag{41}$$

where $\mathbf{U}$ is the interface velocity. As the interface is assumed to be tangentially immobile:

$$\mathbf{v}_c \cdot \mathbf{t} = U_t = 0 \tag{42}$$

where U_t is the scalar tangential velocity of the interface which is zero for an immobile interface. By inserting the velocity vector decomposed in cylindrical coordinates and the derived tangential vector, the equation results in:

$$\frac{v_r + \frac{1}{2}\frac{\partial h}{\partial r} v_z}{\sqrt{1 + \frac{1}{4}\left(\frac{\partial h}{\partial r}\right)^2}} = 0 \tag{43}$$

The kinematic condition is defined by:

$$\mathbf{v}_c \cdot \mathbf{n} = \mathbf{v}_d \cdot \mathbf{n} = \mathbf{U} \cdot \mathbf{n} \tag{44}$$

which can be simplified in:

$$\mathbf{v}_c \cdot \mathbf{n} = U_n \tag{45}$$

since the mass balance across the interface suggests continuity between the normal speed of the interface and the normal component of the film velocity, U_n, the scalar normal velocity of the interface, is not nearly zero this time. The kinematic condition becomes:

$$\mathbf{v}_c \cdot \mathbf{n} = \frac{1}{2}\frac{\partial h}{\partial t} \tag{46}$$

By inserting the decomposed velocity vector and the derived normal vector, the kinematic condition can be expressed as:

$$\frac{v_z - \frac{1}{2}\frac{\partial h}{\partial r} v_r}{\sqrt{1 + \frac{1}{4}\left(\frac{\partial h}{\partial r}\right)^2}} = \frac{1}{2}\frac{\partial h}{\partial t} \tag{47}$$

Both for the no-slip condition and the kinematic condition, the velocities are evaluated at the interface.

A stress balance over the interface can be formulated as:

$$(\mathtt{T}_c \cdot \mathbf{n}) - (\mathtt{T}_d \cdot \mathbf{n}) = (\mathtt{T}_t \cdot \mathbf{n}) \tag{48}$$

where $\mathtt{T}_c$ and $\mathtt{T}_d$ are the total stress tensors in the continuous and dispersed phases and $(\mathtt{T}_t \cdot \mathbf{n})$ represents the discontinuity in stress across the interface. For a rheologically ideal interface, which is studied in this work, the only contribution comes from the surface tension:

$$(\mathtt{T}_t \cdot \mathbf{n}) = 2H\sigma\mathbf{n} \tag{49}$$

where H is the mean curvature which is as well a function of r and t, and σ is the surface tension. Normal and tangential components of the stress balance can further be expressed as:

$$(\mathtt{T}_c : \mathbf{nn}) - (\mathtt{T}_d : \mathbf{nn}) = 2H\sigma\,(\mathbf{n} \cdot \mathbf{n}) \tag{50}$$

Here, $\mathtt{T}_c$ is given by:

$$\mathtt{T}_c = -P_c\mathtt{I} - \mu\left[\nabla\mathbf{v} + (\nabla\mathbf{v})^T\right] \tag{51}$$

where the term in the brackets is defined as the shear rate tensor and the entire second term represents the viscous stress tensor. Here, the identity tensor $\mathtt{I}$ is equal to $\mathtt{I} = \mathbf{e}_r\mathbf{e}_r + \mathbf{e}_\theta\mathbf{e}_\theta + \mathbf{e}_z\mathbf{e}_z$. The gradient of the velocity vector is written as:

$$\nabla\mathbf{v} = \mathbf{e}_r\frac{\partial}{\partial r}\left(v_r\mathbf{e}_r + v_z\mathbf{e}_z\right) + \frac{1}{r}\mathbf{e}_\theta\frac{\partial}{\partial\theta}\left(v_r\mathbf{e}_r + v_z\mathbf{e}_z\right) + \mathbf{e}_z\frac{\partial}{\partial z}\left(v_r\mathbf{e}_r + v_z\mathbf{e}_z\right) \tag{52}$$

The product rule and the relations of derivatives of unit base vectors may be used to simplify the equation to:

$$\nabla\mathbf{v} = \mathbf{e}_r\mathbf{e}_r\frac{\partial v_r}{\partial r} + \mathbf{e}_r\mathbf{e}_z\frac{\partial v_z}{\partial r} + \mathbf{e}_\theta\mathbf{e}_\theta\frac{v_r}{r} + \mathbf{e}_z\mathbf{e}_r\frac{\partial v_r}{\partial z} + \mathbf{e}_z\mathbf{e}_z\frac{\partial v_z}{\partial z} \tag{53}$$

By switching the unit base vectors' order, it is possible to get the transpose of the gradient of the velocity vector:

$$(\nabla\mathbf{v})^T = \mathbf{e}_r\mathbf{e}_r\frac{\partial v_r}{\partial r} + \mathbf{e}_z\mathbf{e}_r\frac{\partial v_z}{\partial r} + \mathbf{e}_\theta\mathbf{e}_\theta\frac{v_r}{r} + \mathbf{e}_r\mathbf{e}_z\frac{\partial v_r}{\partial z} + \mathbf{e}_z\mathbf{e}_z\frac{\partial v_z}{\partial z} \tag{54}$$

These equations can now be used to express the shear rate tensor as:

$$\left[\nabla \mathbf{v} + (\nabla \mathbf{v})^T\right] = 2\mathbf{e}_r\mathbf{e}_r \frac{\partial v_r}{\partial r} + (\mathbf{e}_r\mathbf{e}_z + \mathbf{e}_z\mathbf{e}_r)\frac{\partial v_z}{\partial r} + 2\frac{v_r}{r}\mathbf{e}_\theta\mathbf{e}_\theta + (\mathbf{e}_r\mathbf{e}_z + \mathbf{e}_z\mathbf{e}_r)\frac{\partial v_r}{\partial z} + 2\mathbf{e}_z\mathbf{e}_z\frac{\partial v_z}{\partial z} \tag{55}$$

The normal component of the stress balance is obtained by inserting Eq. 55 into Eq. 51, and employing the definition of dot product of unit base vectors. The normal component of the first term of Eq. 48 reduces to:

$$(\mathtt{T}_c : \mathbf{nn}) = -P_c - \frac{\mu}{1 + \frac{1}{4}\left(\frac{\partial h}{\partial r}\right)^2}\left[\frac{1}{2}\frac{\partial v_r}{\partial r}\left(\frac{\partial h}{\partial r}\right)^2 - \frac{\partial v_z}{\partial r}\frac{\partial h}{\partial r} - \frac{\partial v_r}{\partial z}\frac{\partial h}{\partial r} + 2\frac{\partial v_z}{\partial z}\right] \tag{56}$$

Due to the assumption of gentle collision, the viscous stresses are considered insignificant in the dispersed phase; as a result, the second term in the normal stress balance becomes:

$$(\mathtt{T}_d : \mathbf{nn}) = -P_d \tag{57}$$

The curvature, $2H$, is defined as:

$$2H = \frac{1}{2r}\frac{\partial}{\partial r}\left(r\frac{\partial h}{\partial r}\right) \tag{58}$$

Now, the normal stress balance 48 may be expressed as follows:

$$-P_c - \frac{\mu}{1 + \frac{1}{4}\left(\frac{\partial h}{\partial r}\right)^2}\left[\frac{1}{2}\frac{\partial v_r}{\partial r}\left(\frac{\partial h}{\partial r}\right)^2 - \frac{\partial v_z}{\partial r}\frac{\partial h}{\partial r} - \frac{\partial v_r}{\partial z}\frac{\partial h}{\partial r} + 2\frac{\partial v_z}{\partial z}\right] + P_d = \frac{1}{2r}\frac{\partial}{\partial r}\left(r\frac{\partial h}{\partial r}\right)\sigma \tag{59}$$

2.1.3 Non-Dimensionalization

The given equations can be simplified by reducing them to dimensionless form. A dimensionless variable, $\tilde{x}$, is defined as:

$$\tilde{x} = \frac{x}{\bar{x}} \tag{60}$$

Here, x is a generic variable with dimension, and $\bar{x}$ is its characteristic scale with the corresponding dimension. First, characteristic scales must be introduced for the system of interest. Due to the dimensions of the film, the lubrication theory is applicable. In a thin film the length scales are significantly different, in this particular setting the film radius being much larger than its thickness:

$$\frac{\bar{h}}{\bar{r}} = \epsilon << 1 \tag{61}$$

Here, ϵ is a dimensionless number whose value is unknown. Here it is used as a tool to simplify equations for a better understanding of how magnitudes of different terms compare to each other. Later on in the analysis, after the dominant terms in each equation are determined, the unknown factor ϵ will be omitted from the characteristic scales.

The notion of the gentle collision leading to the formation of a thin film reveals a relationship between the three length scales, as suggested by Ozan and Jakobsen (2019a):

$$\bar{h} << \bar{r} << R_p \tag{62}$$

where $\bar{h}$ and $\bar{r}$ are measures of the thickness and the width of the film, respectively. The characteristic radial length scale of the thin film, $\bar{r}$, and the characteristic axial length scale, $\bar{h}$, are then assumed to be related to the equivalent radius, R_p, as follows:

$$\bar{h} = \epsilon^2 R_p; \qquad \bar{r} = \epsilon R_p \tag{63}$$

Characteristic scales are employed in the form:

$$\bar{P} = \frac{\sigma}{R_p} \quad \bar{h} = \epsilon^2 R_p \quad \bar{r} = \epsilon R p \quad \bar{v_r} = \frac{\epsilon^3\sigma}{\mu} \quad \bar{v_z} = \frac{\epsilon^4\sigma}{\mu} \quad \bar{t} = \frac{R_p\mu}{\epsilon^2\sigma} \tag{64}$$

and by using them, the equations obtained from the previous chapter, 2.1.1 are nondimensionalized and transformed as follows.

First, the continuity equation presented in Eq. 10 is written in dimensionless form as:

$$\frac{1}{\tilde{r}}\frac{\partial}{\partial \tilde{r}}(\tilde{r}\tilde{v}_r) + \frac{\partial \tilde{v}_z}{\partial \tilde{z}} = 0 \tag{65}$$

From Eq. 29, the radial component of the equation of motion is non-dimensionalized as follows:

$$\epsilon^2 Re\left[\frac{\partial \tilde{v}_r}{\partial \tilde{t}}+\frac{1}{\tilde{r}}\frac{\partial}{\partial \tilde{r}}\left(\tilde{r}\tilde{v}_r\tilde{v}_r\right)+\frac{\partial}{\partial \tilde{z}}\left(\tilde{v}_z\tilde{v}_r\right)\right]=-\frac{\partial \tilde{P}}{\partial \tilde{r}}+\left[\frac{\partial}{\partial \tilde{z}}\left(\frac{\partial \tilde{v}_r}{\partial \tilde{z}}\right)\right] \tag{66}$$

where Reynolds number is $Re=\rho\frac{\bar{v}_r\bar{r}}{\mu}$. Comparing the magnitudes of the viscous terms, it is concluded that the final term is much larger than the others, this is why is the only viscous term left in the dimensionless form of the equation. The physics of the problem dictates that the pressure gradient term and the viscous term should be of the same order of magnitude. Otherwise, the approach of the particles would not result in the drainage of the film. And since the collision is gentle and very slow, $Re << 1$, the first term in the equation is significantly small compared to the other two. The dimensionless radial component of the equation of motion appears to be then:

$$0=-\frac{\partial \tilde{P}}{\partial \tilde{r}}+\frac{\partial^2 \tilde{v}_r}{\partial \tilde{z}^2} \tag{67}$$

The z-component of the equation of motion presented in Eq. 29 can be nondimensionalized as:

$$\epsilon^2 Re\left[\frac{\partial \tilde{v}_z}{\partial \tilde{t}}+\frac{1}{\tilde{r}}\frac{\partial}{\partial r}\left(\tilde{v}_r\tilde{v}_z\right)+\frac{\partial}{\partial \tilde{z}}\left(\tilde{v}_z\tilde{v}_z\right)\right]=-\frac{1}{\epsilon^2}\frac{\partial \tilde{P}}{\partial \tilde{z}}+\left[\frac{\partial}{\partial \tilde{r}}\left(\frac{\partial \tilde{v}_r}{\partial \tilde{z}}\right)+\frac{\partial}{\partial \tilde{z}}\left(2\frac{\partial \tilde{v}_z}{\partial \tilde{z}}\right)\right] \tag{68}$$

Since the second term is bigger than the other two, as $\frac{1}{\epsilon^2} >> 1$ and $\frac{1}{\epsilon^2} >> \epsilon^2 Re$, the final dimensionless equation for the axial component is:

$$\frac{\partial \tilde{P}}{\partial \tilde{z}}=0 \tag{69}$$

meaning that the pressure difference along the z-axis can be assumed constant. Again as for the $r-$component of the momentum equation, the inertial term containing the Reynolds number can be assumed negligible, while due to a magnitude comparison, on the left side of the equation only the pressure term along the $z-$axis matters.

The kinematic condition Eq. 47 is non-dimensionalized. Employing the relation in Eq.64 gives:

$$\frac{\epsilon\bar{v}_r\tilde{v}_z-\frac{1}{2}\frac{\epsilon\bar{r}\bar{v}_r}{\bar{r}}\frac{\partial \tilde{h}}{\partial \tilde{r}}\tilde{v}_r}{\sqrt{1+\frac{1}{4}\frac{\epsilon^2\bar{r}^2}{\bar{r}^2}\left(\frac{\partial \tilde{h}}{\partial \tilde{r}}\right)^2}}=\frac{1}{2}\frac{\epsilon\bar{r}}{\bar{t}}\frac{\partial \tilde{h}}{\partial \tilde{t}} \tag{70}$$

The second term inside the square root is negligible since ϵ^2 is a very small term, hence, the denominator is simplified to 1. By inserting the time scale,

$$\bar{t}=\frac{R_p\mu}{\epsilon^2\sigma}=\frac{\bar{r}}{\bar{v}_r} \tag{71}$$

and by grouping the coefficients together, the equation will end up as:

$$\tilde{v}_z-\frac{1}{2}\frac{\partial \tilde{h}}{\partial \tilde{r}}\tilde{v}_r=\frac{1}{2}\frac{\partial \tilde{h}}{\partial \tilde{t}} \tag{72}$$

Since the particles are approaching each other in the system, the position of the interface must change with time, which indicates that the velocity term and the right-hand-side should be comparable.

Moreover, by applying the relations in Eq. 60 and 64 on the no-slip condition, and treating the denominator in the same way as done as for the kinematic condition, the equation results in:

$$\tilde{v}_r+\epsilon^2\frac{1}{2}\frac{\partial \tilde{h}}{\partial \tilde{r}}\tilde{v}_z=0 \tag{73}$$

By comparison of magnitude, the second term is assumed to be negligible because it is multiplied by a very small term, ϵ^2. Thus, the dimensionless no-slip condition assumes the following form:

$$\tilde{v}_r=0 \tag{74}$$

Furthermore, upon substitution of the variables in Eq. 64, the normal stress balance is written in terms of dimensionless variables as:

$$\begin{aligned}-\frac{\mu\bar{v}_r}{\epsilon^3 R_p}\left(\tilde{P}_c-\tilde{P}_d\right)-\frac{\mu}{1+\frac{1}{4}\epsilon^2\left(\frac{\partial \tilde{h}}{\partial \tilde{r}}\right)^2}\left[\frac{1}{2}\frac{\epsilon\bar{v}_r}{R_p}\frac{\partial \tilde{v}_r}{\partial \tilde{r}}\left(\frac{\partial \tilde{h}}{\partial \tilde{r}}\right)^2-\right.\\ \left.\frac{\epsilon\bar{v}_r}{R_p}\frac{\partial \tilde{v}_z}{\partial \tilde{r}}\frac{\partial \tilde{h}}{\partial \tilde{r}}-\frac{\bar{v}_r}{\epsilon R_p}\frac{\partial \tilde{v}_r}{\partial \tilde{z}}\frac{\partial \tilde{h}}{\partial \tilde{r}}+2\frac{\bar{v}_r}{\epsilon R_p}\frac{\partial \tilde{v}_z}{\partial \tilde{z}}\right]=\frac{1}{R_p}\frac{1}{2\tilde{r}}\frac{\partial}{\partial \tilde{r}}\left(\tilde{r}\frac{\partial \tilde{h}}{\partial \tilde{r}}\right)\sigma\end{aligned} \tag{75}$$

The second term on the denominator of the viscous term is surely negligible, as well as for the first two terms inside the square brackets because of the presence of ϵ^2. By grouping all the coefficients and comparing:

$$-\left(\tilde{P}_c - \tilde{P}_d\right) - \epsilon^2 \left[-\frac{\partial \tilde{v}_r}{\partial \tilde{z}}\frac{\partial \tilde{h}}{\partial \tilde{r}} + 2\frac{\partial \tilde{v}_z}{\partial z}\right] = \frac{\epsilon^3 \sigma}{\mu \bar{v}_r}\frac{1}{2\tilde{r}}\frac{\partial}{\partial \tilde{r}}\left(\tilde{r}\frac{\partial \tilde{h}}{\partial \tilde{r}}\right) \tag{76}$$

The second term disappears because it has a smaller dimension compared to the other two due to the presence of ϵ^2. The right-hand-side of the equation represents the interface's ability to deform and must be kept to accurately model phenomena such as dimple formation. Otherwise, without that term the particle will always stay perfectly spherical. The dimensionless normal stress balance equation is then:

$$\tilde{P}_d - \tilde{P}_c = \frac{1}{2r}\frac{\partial}{\partial \tilde{r}}\left(\tilde{r}\frac{\partial \tilde{h}}{\partial \tilde{r}}\right) \tag{77}$$

The equation can be further manipulated to write it in terms of excess pressure defined as the pressure difference between a deformed interface and a perfectly spherical interface. For a perfect sphere the Young-Laplace equation states:

$$\tilde{P}_{d,0} - \tilde{P}_{c,0} = \frac{2\sigma}{R_p} \tag{78}$$

where the subscript 0 stands for a perfectly spherical particle. By employing the definition of dimensionless variable shown in Eq. 60, the equation can be reduced in dimensionless form:

$$\bar{P}(\tilde{P}_{d,0} - \tilde{P}_{c,0}) = \frac{2\sigma}{R_p} \tag{79}$$

And grouping all the constant coefficients:

$$\frac{\bar{P}R_p}{\sigma}(\tilde{P}_d - \tilde{P}_c) = 2 \tag{80}$$

gives the pressure scale shown in Eq. 64. The Young-Laplace equation for a perfect sphere in dimensionless forms then will be:

$$\tilde{P}_{d,0} - \tilde{P}_{c,0} = 2 \tag{81}$$

By subtracting the dimensionless normal stress balance, Eq. 77 from Eq. 81, the following equation is obtained:

$$(\tilde{P}_c - \tilde{P}_{c,0}) - (\tilde{P}_d - \tilde{P}_{d,0}) = 2 - \frac{1}{2r}\frac{\partial}{\partial \tilde{r}}\left(\tilde{r}\frac{\partial \tilde{h}}{\partial \tilde{r}}\right) \tag{82}$$

The second term, $(\tilde{P}_d - \tilde{P}_{d,0})$, is negligible since the pressure change in the continuous phase is expected to be much larger than the change in the dispersed phase. Then, the term $(\tilde{P}_c - \tilde{P}_{c,0})$ represents the excess pressure, $\hat{P}$, which is the difference in pressure in the bulk phase in comparison with the initial spherical one. The final dimensionless normal stress balance becomes:

$$\hat{P} = 2 - \frac{1}{2\tilde{r}}\frac{\partial}{\partial \tilde{r}}\left(\tilde{r}\frac{\partial \tilde{h}}{\partial \tilde{r}}\right) + \frac{A^*}{\tilde{h}^3} \tag{83}$$

where A^* is the dimensionless Hamaker constant, defined by:

$$A^* = \frac{A}{6\pi R_p^2 \sigma} \tag{84}$$

which is added for convention to account for the attractive van der Waals forces. This constant is essential to take into account in order to make coalescence feasible.

2.1.4 Analytical solution of the model

The final equations obtained in the previous section can now be solved partially analytically. The first equation that is integrated is the momentum equation along the r-component, Eq. 67. The z- component of the momentum balance shows that pressure is not a function of z. And then solution of the r-component becomes:

$$\begin{aligned} \frac{\partial^2 \tilde{v}_r}{\partial \tilde{z}^2} &= \frac{\partial \tilde{P}}{\partial \tilde{r}} \\ \frac{\partial}{\partial z}\left(\frac{\partial \tilde{v}_r}{\partial \tilde{z}}\right) &= \frac{\partial \tilde{P}}{\partial \tilde{r}} \\ \frac{\partial \tilde{v}_r}{\partial \tilde{z}} &= \frac{\partial \tilde{P}}{\partial \tilde{r}}\tilde{z} + C_1 \end{aligned} \tag{85}$$

To assign a value to the constant C_1, a boundary condition must be applied. Here, the symmetry condition is used:

$$at \quad \tilde{z} = 0: \quad \frac{\partial \tilde{v}_r}{\partial \tilde{z}} = 0 \tag{86}$$

By employing this boundary condition into Eq. 85, C_1 must be equal to 0. The equation is further integrated:

$$\tilde{v}_r = \frac{\partial \tilde{P}}{\partial \tilde{r}} \frac{\tilde{z}^2}{2} + C_2 \tag{87}$$

Now, to assign a value for the constant C_2 the no-slip condition is applied:

$$at \quad \tilde{z} = \frac{\tilde{h}}{2}: \quad \tilde{v}_r = 0 \tag{88}$$

By substituting into Eq. 87, the constant assumes the value:

$$C_2 = -\frac{\partial \tilde{P}}{\partial \tilde{r}} \frac{\tilde{h}^2}{4} = -\frac{\partial \tilde{P} \tilde{h}^2}{8\tilde{r}} \tag{89}$$

The analytical solution for the r-component of the equation of motion is:

$$\tilde{v}_r = \frac{1}{2} \frac{\partial \tilde{P}}{\partial \tilde{r}} (\tilde{z}^2 - \frac{\tilde{h}^2}{4}) \tag{90}$$

The obtained solution for the $\tilde{v}_r$ can be inserted into the dimensionless continuity equation, Eq. 65, in order to find an analytical solution for the variable $\tilde{v}_z$:

$$\frac{1}{\tilde{r}} \frac{\partial}{\partial \tilde{r}} \left(\tilde{r} \frac{1}{2} \frac{\partial \tilde{P}}{\partial \tilde{r}} (\tilde{z}^2 - \frac{\tilde{h}^2}{4}) \right) + \frac{\partial \tilde{v}_z}{\partial \tilde{z}} = 0 \tag{91}$$

Integrating with respect of dz:

$$\begin{aligned} \frac{\partial \tilde{v}_z}{\partial \tilde{z}} &= -\frac{1}{\tilde{r}} \frac{\partial}{\partial \tilde{r}} \left(\tilde{r} \frac{1}{2} \frac{\partial \tilde{P}}{\partial \tilde{r}} (\tilde{z}^2 - \frac{\tilde{h}^2}{4}) \right) \\ \tilde{v}_z &= -\frac{1}{\tilde{r}} \frac{\partial}{\partial \tilde{r}} \left(\tilde{r} \frac{1}{2} \frac{\partial \tilde{P}}{\partial \tilde{r}} \right) \frac{\tilde{z}^3}{3} + \frac{1}{\tilde{r}} \frac{\partial}{\partial \tilde{r}} \left(\tilde{r} \frac{1}{2} \frac{\partial \tilde{P}}{\partial \tilde{r}} \left(\frac{\tilde{h}^2}{4} \right) \tilde{z} \right) + C_3 \end{aligned} \tag{92}$$

The following boundary condition, from the symmetry condition, is applied to find a solution for the constant C_3:

$$at \quad \tilde{z} = 0: \quad \tilde{v}_Z = 0 \tag{93}$$

From this condition, the value of the constant C_3 must be equal to zero. The analytical solution for $\tilde{v}_z$ is:

$$\tilde{v}_z = -\frac{1}{\tilde{r}} \frac{\partial}{\partial \tilde{r}} \left(\tilde{r} \frac{1}{2} \frac{\partial \tilde{P}}{\partial \tilde{r}} \right) \frac{\tilde{z}^3}{3} + \frac{1}{\tilde{r}} \frac{\partial}{\partial \tilde{r}} \left(\tilde{r} \frac{1}{2} \frac{\partial \tilde{P}}{\partial \tilde{r}} \left(\frac{\tilde{h}^2}{4} \right) \tilde{z} \right) \tag{94}$$

The obtained solutions for the velocities can be inserted into the kinematic condition Eq. 72:

$$\begin{aligned} \frac{1}{2} \frac{\partial \tilde{h}}{\partial \tilde{t}} &= \tilde{v}_z - \frac{1}{2} \frac{\partial \tilde{h}}{\partial \tilde{r}} \tilde{v}_r \\ &= -\frac{1}{\tilde{r}} \frac{\partial}{\partial \tilde{r}} \left(\tilde{r} \frac{\partial \tilde{P}}{2\partial \tilde{r}} \right) \frac{\tilde{z}^3}{3} + \frac{1}{\tilde{r}} \frac{\partial}{\partial \tilde{r}} \left(\tilde{r} \frac{\partial \tilde{P}}{2\partial \tilde{r}} \left(\frac{\tilde{h}^2}{4} \right) \tilde{z} \right) - \frac{\partial \tilde{P}}{2\partial \tilde{r}} (\tilde{z}^2 - \frac{\tilde{h}^2}{4}) \end{aligned} \tag{95}$$

The equation is valid at the interface, at $z = \tilde{h}/2$. By substituting all the z with this interface value:

$$\begin{aligned} \frac{1}{2} \frac{\partial \tilde{h}}{\partial \tilde{t}} &= -\frac{1}{\tilde{r}} \frac{\partial}{\partial \tilde{r}} \left(\tilde{r} \frac{\partial \tilde{P}}{2\partial \tilde{r}} \right) \frac{1}{3} \frac{\tilde{h}^3}{8} + \frac{1}{\tilde{r}} \frac{\partial}{\partial \tilde{r}} \left(\tilde{r} \frac{\partial \tilde{P}}{2\partial \tilde{r}} \left(\frac{\tilde{h}^2}{4} \right) \frac{\tilde{h}}{2} \right) - \cancel{\frac{\partial \tilde{P}}{2\partial \tilde{r}} (\frac{\tilde{h}^2}{4} - \frac{\tilde{h}^2}{4})} \\ &= -\frac{1}{\tilde{r}} \frac{\partial}{\partial \tilde{r}} \left(\tilde{r} \frac{\partial \tilde{P}}{2\partial \tilde{r}} \right) \frac{\tilde{h}^3}{24} + \frac{1}{\tilde{r}} \frac{\partial}{\partial \tilde{r}} \left(\tilde{r} \frac{\partial \tilde{P}}{2\partial \tilde{r}} \left(\frac{\tilde{h}^2}{4} \right) \frac{\tilde{h}}{2} \right) \end{aligned} \tag{96}$$

By employing the chain rule for derivation and significantly manipulating, the equation can be rewritten in a more compact form as:

$$\frac{1}{2} \frac{\partial \tilde{h}}{\partial \tilde{t}} = \frac{1}{24\tilde{r}} \frac{\partial}{\partial \tilde{r}} \left(\tilde{r} \frac{\partial \tilde{P}}{\partial \tilde{r}} \tilde{h}^3 \right) \tag{97}$$

It is not possible to solve Eq. 97 further analytically, and it will be solved simultaneously with the pressure equation, Eq. 83, numerically.

2.2 Power Law

The derived model will now be extended to account for the non-Newtonian continuous phase. An empirical expression is applied to express the stress tensor where the viscosity is considered a function of the magnitude of the shear rate tensor. The model chosen in this study is the power law. The equations remain the same apart from the ones depending on the viscous term: the radial and axial component of the equation of motion and the normal stress balance. In all three equations the viscous term appears but actually, this term is significant only in the r-component of the momentum equation: here, the derivative of the viscosity term appears. And furthermore, in the normal stress balance, no derivative of the stress term is present. Through the text, in order to identify the non-Newtonian viscosity, a new symbol is introduced: η is adopted instead of the Newtonian continuous phase viscosity μ. In order to solve these equations numerically, this derivation seeks to extract the pressure equation and the thinning equation.

2.2.1 Dimensionless Equations

For the non-Newtonian scenario, the viscosity is non-constant. It is worth noting that only the equation of motion and the stress balance are impacted by this modification. The other equations are therefore unaltered. However, only the r-component of the equation of motion, Eq. 29, takes the derivative of viscosity; the other two equations are left essentially unaltered, and the Newtonian viscosity may be replaced with the non-Newtonian one. The r-component then becomes:

$$\begin{aligned} \rho\left[\frac{\partial v_r}{\partial t}+\frac{1}{r}\frac{\partial}{\partial r}\left(r v_r v_r\right)+\frac{\partial}{\partial z}\left(v_z v_r\right)\right]= \\ -\frac{\partial P}{\partial r}+\frac{1}{r}\frac{\partial}{\partial r}\left(2\eta r\frac{\partial v_r}{\partial r}\right)-2\eta\frac{v_r}{r}-\frac{\partial}{\partial z}\left[-\eta\left(\frac{\partial v_z}{\partial r}+\frac{\partial v_r}{\partial z}\right)\right] \end{aligned} \tag{98}$$

As with the Newtonian model, the non-Newtonian model may be simplified by making the equations dimensionless. In order to do so, the characteristic scales already found will be employed as for the Newtonian model, except here, instead of the Newtonian viscosity coefficient μ, a new characteristic scale, $\bar{\eta}$, should be used, which value will be introduces in the following chapter. Non-dimensionalizing the r-component of the equation of motion, yields:

$$\begin{aligned} \rho\frac{\bar{v}_r^2}{\bar{r}}\left[\frac{\partial \tilde{v}_r}{\partial \tilde{t}}+\frac{1}{\tilde{r}}\frac{\partial}{\partial \tilde{r}}\left(\tilde{r}\tilde{v}_r\tilde{v}_r\right)+\frac{\partial}{\partial z}\left(\tilde{v}_z\tilde{v}_r\right)\right]= \\ -\frac{\bar{\eta}\bar{v}_r}{\epsilon^2\bar{r}^2}\frac{\partial \tilde{P}}{\partial \tilde{r}}+\frac{\bar{\eta}\bar{v}_r}{\bar{r}^2}\frac{1}{\tilde{r}}\frac{\partial}{\partial \tilde{r}}\left(2\eta\tilde{r}\frac{\partial \tilde{v}_r}{\partial \tilde{r}}\right)-2\frac{\bar{\eta}\bar{v}_r}{\bar{r}^2}\eta\frac{\tilde{v}_r}{\tilde{r}}+\frac{\bar{\eta}}{\epsilon\bar{r}}\frac{\partial}{\partial \tilde{z}}\left[\eta\left(\frac{\epsilon\bar{v}_r}{\bar{r}}\frac{\partial \tilde{v}_z}{\partial \tilde{r}}+\frac{\bar{v}_r}{\epsilon\bar{r}}\frac{\partial \tilde{v}_r}{\partial \tilde{z}}\right)\right] \end{aligned} \tag{99}$$

As done for the Newtonian model, by comparing the magnitudes of the viscous terms, it is concluded that the final term is much larger than the others, since $\bar{v}_r/\bar{r}^2$ and $\epsilon\bar{h}/\bar{r}$ are much smaller than $\bar{v}_r/\epsilon/\bar{r}$. The viscous term can be rewritten as:

$$\rho\frac{\bar{v}_r^2}{\bar{r}}\left[\frac{\partial \tilde{v}_r}{\partial \tilde{t}}+\frac{1}{\tilde{r}}\frac{\partial}{\partial \tilde{r}}\left(\tilde{r}\tilde{v}_r\tilde{v}_r\right)+\frac{\partial}{\partial \tilde{z}}\left(\tilde{v}_z\tilde{v}_r\right)\right]=-\frac{\bar{\eta}\bar{v}_r}{\epsilon^2\bar{r}^2}\frac{\partial \tilde{P}}{\partial \tilde{r}}+\frac{\bar{\eta}\bar{v}_r}{\epsilon^2\bar{r}^2}\frac{\partial}{\partial \tilde{z}}\left[\eta\frac{\partial \tilde{v}_r}{\partial \tilde{z}}\right] \tag{100}$$

Similar to the Newtonian case, the first term is negligible compared to the pressure and the viscous terms and the final dimensionless non-Newtonian r-component of the momentum equation is:

$$\frac{\partial \tilde{P}}{\partial \tilde{r}}=\frac{\partial}{\partial \tilde{z}}\left[\eta\frac{\partial \tilde{v}_r}{\partial \tilde{z}}\right] \tag{101}$$

This procedure is not repeated for the z-component of the equation of motion as well as for the stress balance because it has already been shown that during the Newtonian non-dimensionalization procedure, the viscous terms in both equations are negligible.

2.2.2 Dimensionless Power law

It is now added the non-Newtonian continuous phase contribution into the obtained model. Since the viscosity for non-Newtonian fluids is considered a function of the magnitude of the shear rate tensor, an empirical model is used to represent the stress tensor. The non-Newtonian fluid is referred to in the context of this model as a generalized Newtonian fluid, and only viscous effects—not elastic ones—are taken into account. This assumption will simplify the derivation of the thinning and pressure equation, making the solver numerically easier. The stress tensor is defined by:

$$\tau=-\eta(\dot{\gamma})\dot{\gamma}=-\eta(\dot{\gamma})\left[\nabla\mathbf{v}+(\nabla\mathbf{v})^T\right] \tag{102}$$

Here, $\dot{\boldsymbol{\gamma}}$ is the shear rate tensor, $\dot{\gamma}$ is the magnitude of $\dot{\boldsymbol{\gamma}}$ and $\eta(\dot{\gamma})$ is the non-Newtonian viscosity. To express this viscosity, the power law is applied:

$$\eta(\dot{\gamma}) = k\dot{\gamma}^{n-1} \tag{103}$$

where k is the flow consistency index and n is the flow behavior index, which correspond to:

- If $0 < n < 1$: shear-thinning fluid
- If $n = 1$: Newtonian fluid
- If $n > 1$: shear-thickening fluid

Inserting the power law gives the following expression for the stress tensor:

$$\tau = -k\dot{\gamma}^{n-1}\left[\nabla\mathbf{v} + (\nabla\mathbf{v})^T\right] \tag{104}$$

where the magnitude of the shear rate tensor, $\dot{\gamma}$, is defined by:

$$\dot{\gamma} = \sqrt{\frac{1}{2}\dot{\boldsymbol{\gamma}} : \dot{\boldsymbol{\gamma}}} \tag{105}$$

The shear rate tensor is given by Eq. 55, and its double dot product with itself gives:

$$\dot{\boldsymbol{\gamma}} : \dot{\boldsymbol{\gamma}} = 4\epsilon^4\frac{\partial v_r}{\partial r}\frac{\partial v_r}{\partial r} + 2\epsilon^6\frac{\partial v_z}{\partial r}\frac{\partial v_z}{\partial r} + 4\epsilon^4\frac{\partial v_z}{\partial r}\frac{\partial v_r}{\partial z} + 2\epsilon^2\frac{\partial v_r}{\partial z}\frac{\partial v_r}{\partial z} + 4\epsilon^4\frac{v_r^2}{r^2} + 4\epsilon^4\frac{\partial v_z}{\partial z}\frac{\partial v_z}{\partial z} \tag{106}$$

In terms of dimensionless variables from Eqs. 64, Eq. 106, becomes:

$$\dot{\boldsymbol{\gamma}} : \dot{\boldsymbol{\gamma}} = \left(\frac{\sigma}{\eta_0 R_p}\right)^2\left[4\epsilon^4\frac{\partial \tilde{v}_r}{\partial \tilde{r}}\frac{\partial \tilde{v}_r}{\partial \tilde{r}} + 2\epsilon^6\frac{\partial \tilde{v}_z}{\partial \tilde{r}}\frac{\partial \tilde{v}_z}{\partial \tilde{r}} + 4\epsilon^4\frac{\partial \tilde{v}_z}{\partial \tilde{r}}\frac{\partial \tilde{v}_r}{\partial z} + 2\epsilon^2\frac{\partial \tilde{v}_r}{\partial z}\frac{\partial \tilde{v}_r}{\partial \tilde{z}} + 4\epsilon^4\frac{\tilde{v}_r^2}{r^2} + 4\epsilon^4\frac{\partial \tilde{v}_z}{\partial \tilde{z}}\frac{\partial \tilde{v}_z}{\partial \tilde{z}}\right] \tag{107}$$

Here, the third last term is determined to be much more significant than all the other terms which therefore are neglected. Hence, the magnitude of the shear rate tensor can be reduced to:

$$\dot{\gamma} = \sqrt{\frac{1}{2}\dot{\boldsymbol{\gamma}} : \dot{\boldsymbol{\gamma}}} \approx \sqrt{\epsilon^2\left(\frac{\sigma}{\eta_0 R_p}\right)^2\frac{\partial \tilde{v}_r}{\partial \tilde{z}}\frac{\partial \tilde{v}_r}{\partial \tilde{z}}} = \left|\frac{\epsilon\sigma}{\eta_0 R_p}\frac{\partial \tilde{v}_r}{\partial \tilde{z}}\right| = \left|\frac{\partial v_r}{\partial z}\right| \tag{108}$$

By inserting the obtained expression for the shear rate tensor into the power law in Eq. 103, and setting the characteristic scale, the power law can be written as:

$$\eta = k\left|\frac{\partial v_r}{\partial z}\right|^{n-1} \tag{109}$$

Only the equations including this component are impacted since the viscous stress tensor is the only factor that differs between the non-Newtonian and Newtonian instances. Thus, only the equations of motion and the stress balance component change, while the other equations stay the same. On the other hand, the form of the equations of motion and the component of the stress balance shouldn't alter as long as the power law isn't included for η and the viscosity isn't considered constant and taken outside any derivatives.

Making the equation dimensionless, as was done for the Newtonian model, the non-Newtonian model is simplified. Characteristic scales employed are the ones shown in Eqs. 64, but now the viscosity coefficient μ for the continuous phase is replaced by a constant non-Newtonian coefficient, η_0:

$$\bar{P} = \frac{\sigma}{R_p} \quad \bar{h} = \epsilon^2 R_p \quad \bar{r} = \epsilon R p \quad \bar{v_r} = \frac{\epsilon^3\sigma}{\eta_0} \quad \bar{v_z} = \frac{\epsilon^4\sigma}{\eta_0} \quad \bar{t} = \frac{R_p\eta_0}{\epsilon^2\sigma} \tag{110}$$

For the non-Newtonian viscosity, the following variable substitution is employed:

$$\eta = \eta_0\tilde{\eta} \tag{111}$$

By non-dimensionalizing the power law given in Eq. 103, the characteristic scale, η_0, can be found as:

$$\eta_0\tilde{\eta} = k\left(\frac{\bar{v}_r}{\bar{h}}\right)^{n-1}\left|\frac{\partial \tilde{v}_r}{\partial \tilde{z}}\right|^{n-1} \tag{112}$$

This gives the following expression for η_0:

$$\eta_0 = k\left(\frac{\bar{v}_r}{\bar{h}}\right)^{n-1} \tag{113}$$

By inserting the characteristic scales for $\bar{v}_r$ and $\bar{h}$, the Eq. 113 is rewritten to:

$$\eta_0 = k\left(\frac{\epsilon^3\sigma}{\epsilon^2\eta_0 R_p}\right)^{n-1} \tag{114}$$

and further rearranged to:

$$\eta_0 = k^{1/n}\left(\frac{\epsilon^2\sigma}{R_p}\right)^{1-1/n} \tag{115}$$

The dimensionless power law can be expressed as follows:

$$\tilde{\eta} = \left|\frac{\partial\tilde{v}_r}{\partial\tilde{z}}\right|^{n-1} \tag{116}$$

2.2.3 Analytical solution with Power law

By adding the Eq. 116 to the previous set of equations, especially to the dimensionless $r-$component of the momentum equation, Eq. 101, they can be rearranged in two main equations like for Newtonian continuous media. By taking the Eq. 101 and inserting the Eq. 116, this can be solved numerically and become:

$$\frac{\partial\tilde{P}}{\partial\tilde{r}} = \frac{\partial}{\partial\tilde{z}}\left[\left(-\frac{\partial\tilde{v}_r}{\partial\tilde{z}}\right)^{n-1}\frac{\partial\tilde{v}_r}{\partial\tilde{z}}\right] \tag{117}$$

$$\frac{\partial\tilde{P}}{\partial\tilde{r}} = -\frac{\partial}{\partial\tilde{z}}\left(-\frac{\partial\tilde{v}_r}{\partial\tilde{z}}\right)^{n} \tag{118}$$

where the sign is fixed due to the assumption of symmetry for $z > 0$. Proceeding by integrating the equation:

$$\frac{\partial\tilde{P}}{\partial\tilde{r}}\tilde{z} = -\left(-\frac{\partial\tilde{v}_r}{\partial\tilde{z}}\right)^{n} + C_1 \tag{119}$$

where C_1 is a constant the value of which can be found due to the assumption of symmetry around the radial axis:

$$at \quad \tilde{z} = 0: \quad \frac{\partial\tilde{v}_r}{\partial\tilde{z}} = 0 \longrightarrow C_1 = 0 \tag{120}$$

The equation is rearranged as follows:

$$-\left(-\frac{\partial\tilde{P}}{\partial\tilde{r}}\right)^{1/n}\tilde{z}^{1/n} = \frac{\partial\tilde{v}_r}{\partial\tilde{z}} \tag{121}$$

A second integration can be now made:

$$\tilde{v}_r = -\left(-\frac{\partial\tilde{P}}{\partial\tilde{r}}\right)^{1/n}\frac{1}{1/n+1}\tilde{z}^{1/n+1} + C_2 \tag{122}$$

By applying the equation 74, a value to the constant C_2 can be assigned:

$$at \quad \tilde{z} = \frac{\tilde{h}}{2}: \quad \tilde{v}_r = 0 \tag{123}$$

Then by substituting into Eq. 122:

$$0 = -\frac{1}{1/n+1}\left(-\frac{\partial\tilde{P}}{\partial\tilde{r}}\right)^{1/n}\left(\frac{\tilde{h}}{2}\right)^{1/n+1} + C_2 \tag{124}$$

By inserting the found value of C_2 into the Eq. 122 and rearranging, a new expression for the dimensionless velocity along the axial component is found:

$$\tilde{v}_r = \frac{1}{1/n+1}\left(-\frac{\partial\tilde{P}}{\partial\tilde{r}}\right)^{1/n}\left[\left(\frac{\tilde{h}}{2}\right)^{1/n+1} - z^{1/n+1}\right] \tag{125}$$

By inserting this expression into the dimensionless continuity equation, Eq. 65:

$$\frac{1}{\tilde{r}}\frac{\partial}{\partial\tilde{r}}\left(\tilde{r}\frac{1}{1/n+1}\left(-\frac{\partial\tilde{P}}{\partial\tilde{r}}\right)^{1/n}\left[\left(\frac{\tilde{h}}{2}\right)^{1/n+1}-\tilde{z}^{1/n+1}\right]\right)=-\frac{\partial\tilde{v}_z}{\partial\tilde{z}} \tag{126}$$

By integrating, another constant C_3 is added to the equation:

$$\tilde{v}_z=\frac{1}{\tilde{r}}\frac{\partial}{\partial\tilde{r}}\left[\tilde{r}\frac{1}{1/n+1}\left(-\frac{\partial\tilde{P}}{\partial\tilde{r}}\right)^{1/n}\left(\frac{\tilde{h}}{2}\right)^{1/n+1}\right]z-\frac{1}{\tilde{r}}\frac{\partial}{\partial\tilde{r}}\left(\tilde{r}\frac{1}{1/n+1}\left(-\frac{\partial\tilde{P}}{\partial\tilde{r}}\right)^{1/n}\right)\frac{1}{1/n+2}z^{1/n+2}+C_3 \tag{127}$$

The constant C_3 is solved this time by using again the consition of symmetry around the radial axis:

$$at\quad \tilde{z}=0:\quad \tilde{z}=0\longrightarrow C_3=0 \tag{128}$$

And by substituting into the Eq. 127, a new expression for the dimensionless radial component of the velocity for a Power law continuous media is found:

$$\tilde{v}_z=\frac{1}{\tilde{r}}\frac{\partial}{\partial\tilde{r}}\left(\tilde{r}\frac{1}{1/n+1}\left(-\frac{\partial\tilde{P}}{\partial\tilde{r}}\right)^{1/n}\left[\left(\frac{\tilde{h}}{2}\right)^{1/n+1}\tilde{z}-\frac{1}{1/n+2}\tilde{z}^{1/n+2}\right]\right) \tag{129}$$

By substituting the expressions of the radial and axial components of the velocity into the dimensionless kinematic condition, Eq. 72, it is possible to proceed similarly as for the Newtonian case:

$$\begin{aligned}\frac{1}{2}\frac{\partial\tilde{h}}{\partial\tilde{t}}=&\frac{1}{\tilde{r}}\frac{\partial}{\partial\tilde{r}}\left(\tilde{r}\frac{1}{1/n+1}\left(-\frac{\partial\tilde{P}}{\partial\tilde{r}}\right)^{1/n}\left[\left(\frac{\tilde{h}}{2}\right)^{1/n+1}\tilde{z}-\frac{1}{1/n+2}\tilde{z}^{1/n+2}\right]\right)\\&+\frac{1}{2}\frac{\partial\tilde{h}}{\partial\tilde{r}}\frac{1}{1/n+1}\left(-\frac{\partial\tilde{P}}{\partial\tilde{r}}\right)^{1/n}\left[\left(\frac{\tilde{h}}{2}\right)^{1/n+1}-z^{1/n+1}\right]\end{aligned} \tag{130}$$

Since this condition is valid only at the interface, $z=h/2$:

$$\frac{1}{2}\frac{\partial\tilde{h}}{\partial\tilde{t}}=\frac{1}{\tilde{r}}\frac{\partial}{\partial\tilde{r}}\left(\tilde{r}\frac{1}{1/n+1}\left(-\frac{\partial\tilde{P}}{\partial\tilde{r}}\right)^{1/n}\left[\left(\frac{\tilde{h}}{2}\right)^{1/n+1}\left(\frac{\tilde{h}}{2}\right)-\frac{1}{1/n+2}\left(\frac{\tilde{h}}{2}\right)^{1/n+2}\right]\right) \tag{131}$$

in accordance with the no-slip condition at the interface, for which $\tilde{v}_r=0$. The equation is manipulated as:

$$\begin{aligned}\frac{1}{2}\frac{\partial\tilde{h}}{\partial\tilde{t}}=&\frac{1}{\tilde{r}}\frac{\partial}{\partial\tilde{r}}\left[\tilde{r}\frac{1}{1/n+1}\left(-\frac{\partial\tilde{P}}{\partial\tilde{r}}\right)^{1/n}\left(\frac{\tilde{h}}{2}\right)^{1/n+1}\right]\left(\frac{\tilde{h}}{2}\right)\\&+\frac{1}{\tilde{r}}\frac{\partial}{\partial\tilde{r}}\left[\tilde{r}\frac{1}{1/n+1}\left(-\frac{\partial\tilde{P}}{\partial\tilde{r}}\right)^{1/n}\right]\end{aligned} \tag{132}$$

and by applying the product rule:

$$\begin{aligned}\frac{1}{2}\frac{\partial\tilde{h}}{\partial\tilde{t}}=&\frac{1}{\tilde{r}}\frac{\partial}{\partial\tilde{r}}\left[\tilde{r}\frac{1}{1/n+1}\left(-\frac{\partial\tilde{P}}{\partial\tilde{r}}\right)^{1/n}\right]\left[\left(\frac{\tilde{h}}{2}\right)^{1/n+2}-\frac{1}{1/n+2}\left(\frac{\tilde{h}}{2}\right)^{1/n+2}\right]\\&-\frac{1}{\tilde{r}}\frac{\partial}{\partial\tilde{r}}\left[\left(\frac{\tilde{h}}{2}\right)^{1/n+1}\right]\tilde{r}\frac{1}{1/n+1}\left(-\frac{\partial\tilde{P}}{\partial\tilde{r}}\right)^{1/n}\left(\frac{\tilde{h}}{2}\right)\end{aligned} \tag{133}$$

By applying the chain rule, the first derivative in the second term on the right-hand-side becomes:

$$\frac{\partial}{\partial\tilde{r}}\left[\left(\frac{\tilde{h}}{2}\right)^{1/n+1}\right]=\left(\frac{1}{n}+1\right)\frac{\partial}{\partial\tilde{r}}\left(\frac{\tilde{h}}{2}\right)\left(\frac{\tilde{h}}{2}\right)^{1/n} \tag{134}$$

The equation becomes:

$$\frac{1}{2}\frac{\partial \tilde{h}}{\partial \tilde{t}} = \frac{1}{\tilde{r}}\frac{\partial}{\partial \tilde{r}}\left[\tilde{r}\frac{1}{1/n+1}\left(-\frac{\partial \tilde{P}}{\partial \tilde{r}}\right)^{1/n}\right]\left(\frac{\tilde{h}}{2}\right)^{1/n+2}\left[\frac{1/n+1}{1/n+2}\right] - \left(\frac{1}{n}+1\right)\frac{\partial}{\partial \tilde{r}}\left(\frac{\tilde{h}}{2}\right)\left(\frac{\tilde{h}}{2}\right)^{1/n}\tilde{r}\frac{1}{1/n+1}\left(-\frac{\partial \tilde{P}}{\partial \tilde{r}}\right)^{1/n}\left(\frac{\tilde{h}}{2}\right) \tag{135}$$

$$\frac{1}{2}\frac{\partial \tilde{h}}{\partial \tilde{t}} = \frac{1}{\tilde{r}}\frac{\partial}{\partial \tilde{r}}\left[\tilde{r}\left(-\frac{\partial \tilde{P}}{\partial \tilde{r}}\right)^{1/n}\right]\left(\frac{\tilde{h}}{2}\right)^{1/n+2}\left[\frac{1}{1/n+2}\right] - \frac{1}{\tilde{r}}\tilde{r}\left(-\left(\frac{\partial \tilde{P}}{\partial \tilde{r}}\right)\right)^{1/n}\left(\frac{\tilde{h}}{2}\right)^{1/n+1}\frac{\partial}{\partial \tilde{r}}\left(\frac{\tilde{h}}{2}\right) \tag{136}$$

By applying the chain rule in reverse on the last term:

$$\left(\frac{1}{n}+2\right)\frac{\partial}{\partial \tilde{r}}\left(\frac{\tilde{h}}{2}\right)\left(\frac{\tilde{h}}{2}\right)^{1/n+1} = \frac{\partial}{\partial \tilde{r}}\left[\left(\frac{\tilde{h}}{2}\right)^{1/n+2}\right] \tag{137}$$

and inserting it into the kinematic equation gives:

$$\frac{1}{2}\frac{\partial \tilde{h}}{\partial \tilde{t}} = \frac{1}{\tilde{r}}\frac{\partial}{\partial \tilde{r}}\left[\tilde{r}\left(-\frac{\partial \tilde{P}}{\partial \tilde{r}}\right)^{1/n}\right]\left(\frac{\tilde{h}}{2}\right)^{1/n+2}\left[\frac{1}{1/n+2}\right] - \frac{1}{\tilde{r}}\tilde{r}\left(-\frac{\partial \tilde{P}}{\partial \tilde{r}}\right)^{1/n}\frac{\partial}{\partial \tilde{r}}\left[\left(\frac{\tilde{h}}{2}\right)^{1/n+2}\right]\frac{1}{1/n+2} \tag{138}$$

After the entire set of equations for a Power law continuous media is solved analytically and manipulated, again, two main equations can be solved numerically to find the solution to the problem. The thinning equation just written up above, rearranged results:

$$\frac{1}{2}\frac{\partial \tilde{h}}{\partial \tilde{t}} = -\frac{1}{2}\frac{\partial}{\partial \tilde{r}}\left(\tilde{r}\left(-\frac{\partial \tilde{P}}{\partial \tilde{r}}\right)^{1/n}\left(\frac{\tilde{h}}{2}\right)^{1/n+2}\right)\frac{1}{1/n+2} \tag{139}$$

and the pressure equation, which is obtained from the stress balance equation exactly as for the Newtonian case, Eq. 83:

$$\hat{P} = 2 - \frac{1}{\tilde{r}}\frac{\partial}{\partial \tilde{r}}\left(\tilde{r}\frac{\partial \tilde{h}}{\partial \tilde{r}}\right) + \frac{A^*}{\tilde{h}^3} \tag{140}$$

The thinning and pressure equations, i.e., Eqs. 139 and 140, are solved simultaneously with the following boundary and initial conditions:

$$\left.\frac{\partial \tilde{h}}{\partial \tilde{r}}\right|_{\tilde{r}=0} = 0; \quad \left.\frac{\partial \tilde{P}}{\partial \tilde{r}}\right|_{\tilde{r}=0} = 0 \tag{141}$$

$$\left.\frac{\partial h}{\partial t}\right|_{\tilde{r}=\tilde{r}_\infty} = -\tilde{V}_{app}(t); \quad \left.\tilde{P}\right|_{\tilde{r}=\tilde{r}_\infty} = 0 \tag{142}$$

Due to the assumption of axisymmetry within the film, the boundary conditions shown in Eq. 141 are used in the present case. Furthermore, it is assumed that at a sufficiently high radial distance, $\tilde{r}_\infty$, the form of the interface and the approach velocity are unaffected by the impact due to the assumption of a gentle collision. Thus, the boundary conditions in Eq. 142 appear. To resemble the film between two initially spherical particles, the initial condition for the film thickness is taken as:

$$\tilde{h}_0 = \tilde{h}_{min,0} + \tilde{r}^2 \tag{143}$$

where $\tilde{h}_{min,0}$ is the dimensionless minimum initial thickness.

2.3 Force Balance

Ozan et al. (2021) studied the film drainage between two fluid particles with deformable interfaces that can support dimple formation by considering a time-dependent relative approach velocity. The time-dependent behavior is governed by a force balance that accounts for the changes in the kinetic and the particle surface energies. When the film's resistance to the drainage is large enough the relative approach velocity can attain negative values, signifying the onset of rebound of the particles. Thus, in addition to predicting coalescence, the

drainage model is able to estimate the rebound as well. The time-dependent behavior of the approach velocity of i^{th} fluid particle is described by a force balance:

$$m_{A,i}\frac{\partial \mathbf{V}_i}{\partial t} = \mathbf{F}_{b,i} + \mathbf{F}_{d,i} + \mathbf{F}_{f,i} \tag{144}$$

where $m_{A,i}$ is the added mass.

$$m_{A,i} = m_i\left(1 + C_m\frac{\rho_c}{\rho_d}\right) \tag{145}$$

$\mathbf{F}_{b,i}$ and $\mathbf{F}_{d,i}$ are the buoyancy and the drag forces acting on the particle, and the film force, $\mathbf{F}_{f,i}$ is the hydrodynamic force resisting the motion of the particle due to the lubrication pressure build up inside the film. By writing the forces explicitly, the equation can be expressed as:

$$m_{A,i}\frac{\partial \mathbf{V}_i}{\partial t} = m_i\left(1 - \frac{\rho_c}{\rho_d}\mathbf{g}\right) - C_{D,i}Re_i\frac{\pi}{4}\mu_c R_i\mathbf{V}_i + \mathbf{d_i}\int_0^{2\pi}\int_0^{r_\infty} rpdrd\sigma \tag{146}$$

$$= m_i\left(1 - \frac{\rho_c}{\rho_d}\mathbf{g}\right) - C_{D,i}Re_i\frac{\pi}{4}\mu_c R_i\mathbf{V}_i + \mathbf{d_i}2\pi\int_0^{r_\infty} rpdr \tag{147}$$

where $C_{D,i}$ and Re_i are the drag coefficient and the instantaneous Reynolds number, respectively. The $\mathbf{d}_i$ term in the film force is added to ensure that the film force always acts in the opposite direction to the approach of the particles. It depends on the orientation of the coordinate system and the position of the fluid particles relative to each other.

The dimensionless version of this equation is:

$$\frac{\partial \tilde{V}_i}{\partial \tilde{t}} = \frac{m_i}{m_{A,i}}\frac{\mu_c^2 Rp}{\sigma^2}\left(1 - \frac{\rho_c}{\rho_d}\right)(\mathbf{g}\cdot\mathbf{k}) - Oh_{A,i}^2\left(C_{D,i}Re_i\frac{\pi}{4}\frac{R_i}{R_p}\tilde{V}_i - d_i 2\pi\int_0^{\tilde{r}_\infty}\tilde{r}\tilde{p}d\tilde{r}\right) \tag{148}$$

where $Oh_{A,i} = \frac{\mu_c Rp}{\sqrt{M_{A,i}\sigma}}$ is an Ohnesorge number defined by considering the added mass of the particles. For the collision involving similar size fluid particles, i.e., $R_1 \approx R_2 \approx R_p$ the equation simplifies to:

$$\frac{\partial \tilde{V}_i}{\partial \tilde{t}} = \frac{m}{m_A}\frac{\mu_c^2 Rp}{\sigma^2}\left(1 - \frac{\rho_c}{\rho_d}\right)(\mathbf{g}\cdot\mathbf{k}) - Oh_A^2\left(C_{D,i}Re_i\frac{\pi}{4}\tilde{V}_i - d_i 2\pi\int_0^{\tilde{r}_\infty}\tilde{r}\tilde{p}d\tilde{r}\right) \tag{149}$$

where the subscripts i are omitted when a quantity is the same for both particles. As the interactions between similar size particles are considered, the buoyancy forces acting on the particles are approximately equal to each other, and their effect on the relative approach velocity, $V_{app} = V_2 - V_1$, is negligible. Therefore, the buoyancy term in the equation is excluded from the calculations. The relative importance of the drag and the film forces, on the other hand, depends significantly on the distance between the particles and the extent of the interfacial deformations. This work aims to study the film dynamics at the interaction of the two particles rather than investigate the earlier stages of the approach, therefore the film force plays a big role while the drag force is found to be less significant, yet not completely negligible. Furthermore, in this work, interfaces have zero degrees of mobility. For the calculation of the drag coefficient, the expression proposed by Schiller and Naumann (1933) is used:

$$C_{D,i} = 24Re_i^{-1}(1 + 0.15Re_i^{0.687}) \tag{150}$$

which is a common empirical equation to use to model particle-particle drag force between fluid phases in Newtonian multiphase systems and so far it shows the best agreements in literature.

2.3.1 Critical Rebound Velocity

The smallest approach velocity that allows rebound is denoted as the critical relative approach velocity V_c of the corresponding parameter set. This value was of crucial importance in order to set a boundary between rebound and the beginning of the coalescence phase. Above it, the rebound process is completed. Below this value, the film ruptures due to the attractive intermolecular forces. This critical velocity here introduced will be important later on in order to validate the model used in this study by comparing previous studies. Furthermore, this parameter is one of the key points of the research to subsequently analyze how other parameters typical of non-Newtonian fluids, like n for example, could affect the simulation. As already mentioned in the previous paragraph, an important factor determining the coalescence characteristics of a collision is the tangential mobility of the fluid particles. In Chapter 4.2 the influence of this assumption will be evaluated.

2.4 Power-law drag effect on a particle

The drag on a sphere is a force of resistance that develops as matter moves through a liquid, and the drag coefficient is a physical quantity that relies on the geometry of the material and the viscosity of the liquid. For these reasons, it is of interest to investigate and compare both the Newtonian and non-Newtonian behavior of the fluid. As the Newtonian case was already considered as the simple scenario, now the drag on a power-law fluid is taken into consideration.

For non-Newtonian fluids, the drag on a falling sphere is affected by the power-law fluid surrounding it. From previous studies, Dazhi and Tanner (2006), such effect is investigated more for shear-thinning fluids, which are more common to find in real-life applications.

2.4.1 Shear-thinning fluids

According to the preponderance of studies on drag on a sphere, the power-law model dominates the theoretical data that is currently available. The likely cause of this is the capability of utilizing the index parameter n to evaluate the significance of the shear-thinning (or shear-thickening) effects in a flow problem. The majority of theoretical discoveries are also based on shear-thinning fluids, which are employed in practical applications the most frequently. In the work of Dazhi and Tanner (1985), the drag F_d on a sphere is presented as:

$$F_d = 6\pi k \left(\frac{V_i}{2R_p}\right)^{n-1} V_i R_p X(n) \tag{151}$$

where the radius R_p is the radius of the sphere moving at speed V_i in an unbounded power-law fluid, with power-law parameter m and index n. Here, the $X(n)$ is a correction parameter accounting for the effect of the power-law viscosity, also named the drag correction factor. When $n = 1$ (Newtonian case), the value of the function X is 1. This equation resembles the one already found for Newtonian fluids, Eq. 146, where similar expression groups can be pointed out: the viscosity term, the linear dependence from the radius, and the velocity. The Newtonian drag force takes into account the inertia with the Reynolds number correction contained in the Cd_i term, while this non-Newtonian equation adds a correction due to the power-law index by adding the parameter $X(n)$. When $n = 1$ (Newtonian case), the value of the correction parameter is equal to 1.

In the current work, the modeling efforts start based on this data. Figure 2 shows the curve fitting obtained from the plot of the numerical calculations of the values of the drag correction factor X from Dazhi and Gu et al. (1985). The values for the drag correction factor X have been found numerically from sphere-in-sphere and

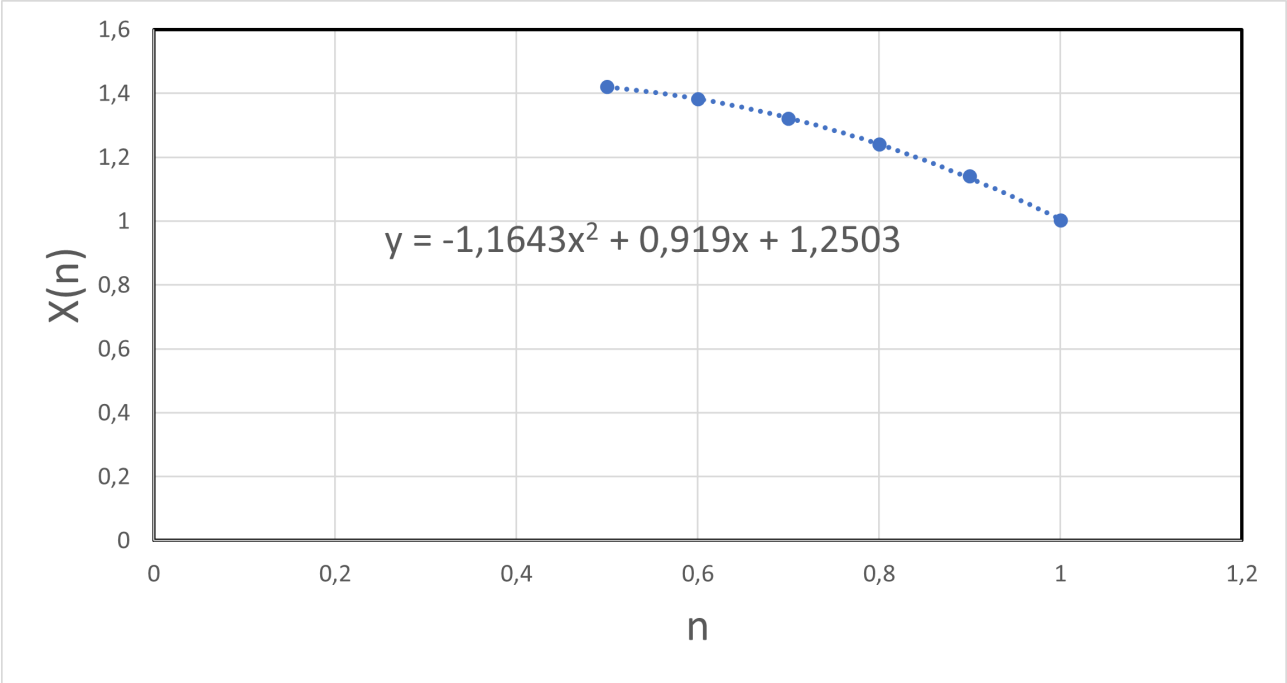

Figure 2: curve fitting of the drag correction factor X for unbounded fluid in a power-law fluid. Data fitting from Dazhi and Gu et al. (1985)

sphere-in-tube configuration experiments to assess the importance of wall effects on the drag force. The trends reveal an increase in the values of X as the values of the index n decrease.

Remembering the viscosity scale showed in Chapter 2.2:

$$\eta_0 = m\left(\frac{\tilde{V}_i}{R_p}\right)^{n-1} \tag{152}$$

and by using the scales shown in the same Chapter, the dimensionless form of Eq. 151 turns out to be:

$$\tilde{F}_d = 6\pi m\left(\frac{\tilde{V}_i}{R_p}\right)^{n-1}\left(\frac{|\tilde{V}_i|_i}{2}\right)^{n-1}\bar{V}_i|\tilde{V}_i|RpX(n) \tag{153}$$

$$= 6\pi\eta_0\left(\frac{|\tilde{V}_i|}{2}\right)^{n-1}\bar{V}_i|\tilde{V}_i|RpX(n) \tag{154}$$

The drag force expression can now be replaced with this new drag expression for power-law fluids in the force balance (Eq. 146), leading to the new following equation for power-law fluids:

$$m_{A,i}\frac{\partial \mathbf{V}_i}{\partial t} = m_i\left(1-\frac{\rho_c}{\rho_d}\mathbf{g}\right) - 6\pi\eta_0\left(\frac{|\tilde{V}_i|}{2}\right)^{n-1}\bar{V}_i|\tilde{V}_i|RpX(n) + \mathbf{d_i}\int_0^{2\pi}\int_0^{r_\infty} rpdrd\sigma \tag{155}$$

Remembering the velocity scale and the time scale introduced in Chap. 2.2, the dimensionless version of this equation is:

$$\frac{\partial \tilde{V}_i}{\partial \tilde{t}} = \frac{m_i}{m_{A,i}}\frac{\mu_c^2 Rp}{\sigma^2}\left(1-\frac{\rho_c}{\rho_d}\right)(\mathbf{g}\cdot\mathbf{k}) - \frac{Rp\eta_0}{\sigma m_{A,i}}6\pi\eta_0\left(\frac{|\tilde{V}_i|}{2}\right)^{n-1}|\tilde{V}_i|RpX(n) + Oh_{A,i}^2\left(d_i 2\pi\int_0^{\tilde{r}_\infty}\tilde{r}\tilde{p}d\tilde{r}\right) \tag{156}$$

Remembering the definition of the Ohnesorge number, $Oh_{A,i} = \frac{\eta_0 Rp}{\sqrt{m_{A,i}\sigma}}$, the parameters in front of the drag term can be grouped together. Considering the collision involving similar size fluid particles, the equation simplifies to:

$$\frac{\partial \tilde{V}_i}{\partial \tilde{t}} = \frac{m}{m_A}\frac{\mu_c^2 Rp}{\sigma^2}\left(1-\frac{\rho_c}{\rho_d}\right)(\mathbf{g}\cdot\mathbf{k}) - Oh_A^2\left(6\pi\left(\frac{|\tilde{V}_i|}{2}\right)^{n-1}|\tilde{V}_i|X(n) - d_i 2\pi\int_0^{\tilde{r}_\infty}\tilde{r}\tilde{p}d\tilde{r}\right) \tag{157}$$

It should be further underlined that the contribution of the buoyancy and film forces is indifferent for Newtonian and non-Newtonian fluids since no viscosity term appears.

2.4.2 Shear-thickening fluids

The motion of spheres in dilatant fluids has only been the subject of a small number of studies. Despite preliminary research on the creeping motion of spheres in power-law fluids with a flow behavior index greater than unity being published by Tomita (1959) and Wallick et al. (1962), as reported in Chhabra et al. (2006), shear thickening fluids are relatively uncommon in industrial applications. The governing equations for power-law fluids flowing across a sphere up to $Re < 100$ and $1 < n < 1.8$ were numerically solved by Tripathi and Chhabra in 1995. The drag correction factor X is strongly influenced by the flow behavior index at low Reynolds numbers, but the impact of n gradually decreases at high Reynolds numbers. The curves shown in Fig 3 are fitted with the experimental values of C_D for spheres in dilatant fluids from Tripathi et al. (2006). In the main simulation, for the calculation of the drag coefficient, the expression for the $C_{D,i}$ was used from Schiller and Naumann (1933), Eq. 150. This equation for the drag formula is well-known and other expressions proposed give the same qualitative drainage behavior with only trivial differences in the V_{app} values observed, like Caylan et al. (2001) or Chhabra and Uhlherr (1980). For these reasons, this equation was used as the model to derive similar-looking formulas for other values of n for dilatant fluids. Keeping in mind the equation proposed by Schiller and Naumann:

$$C_D = 24Re^{-1}(1+0.15Re^{0.687})$$

this type of equation can be derived for other values of drag correction factors and Reynolds numbers:

$$C_D = k|_{Re\to 0}Re^{-1}(1+f(Re)) \tag{158}$$

From the experimental data of the drag correction factor values C_D for spheres in dilatant fluids (Tripathi, A. and Chhabra, (2006)), the values of the $f(Re)$ were obtained using the Eq. 158 and plotted against the Re values. Then a power law type of fitting was made for each n. As it can be seen from Fig. 4 the first curve in power scale is the Newtonian case. The Newtonian case reports parameters that solidly agree with the one proposed by Schiller and Naumann (1933) in Eq. 150. From these results, new expressions for $n = 1.2$ and

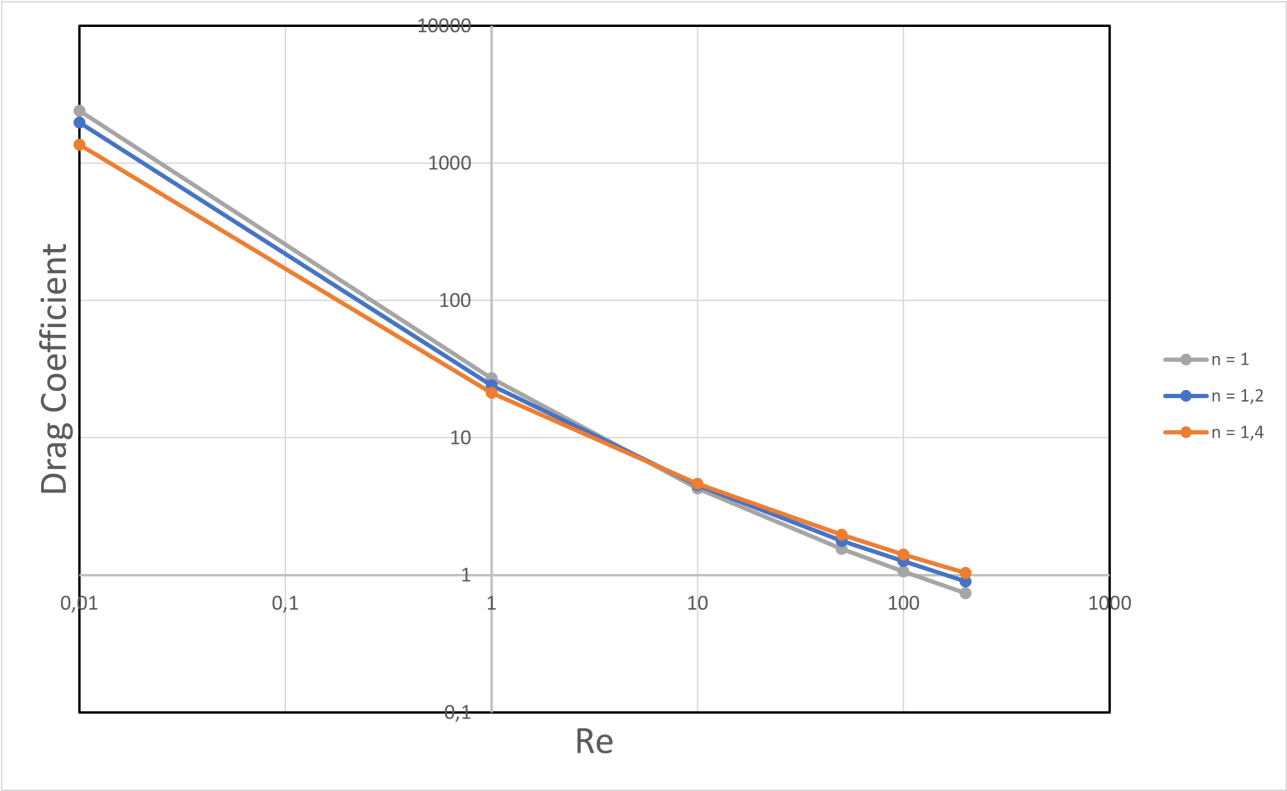

Figure 3: curve fitting of the drag correction factor values C_D for spheres in dilatant fluids. Curves are fitted for different n values: 1 (Newtonian case), 1.2, and 1.4. Raw data from: Tripathi et al. (2006)

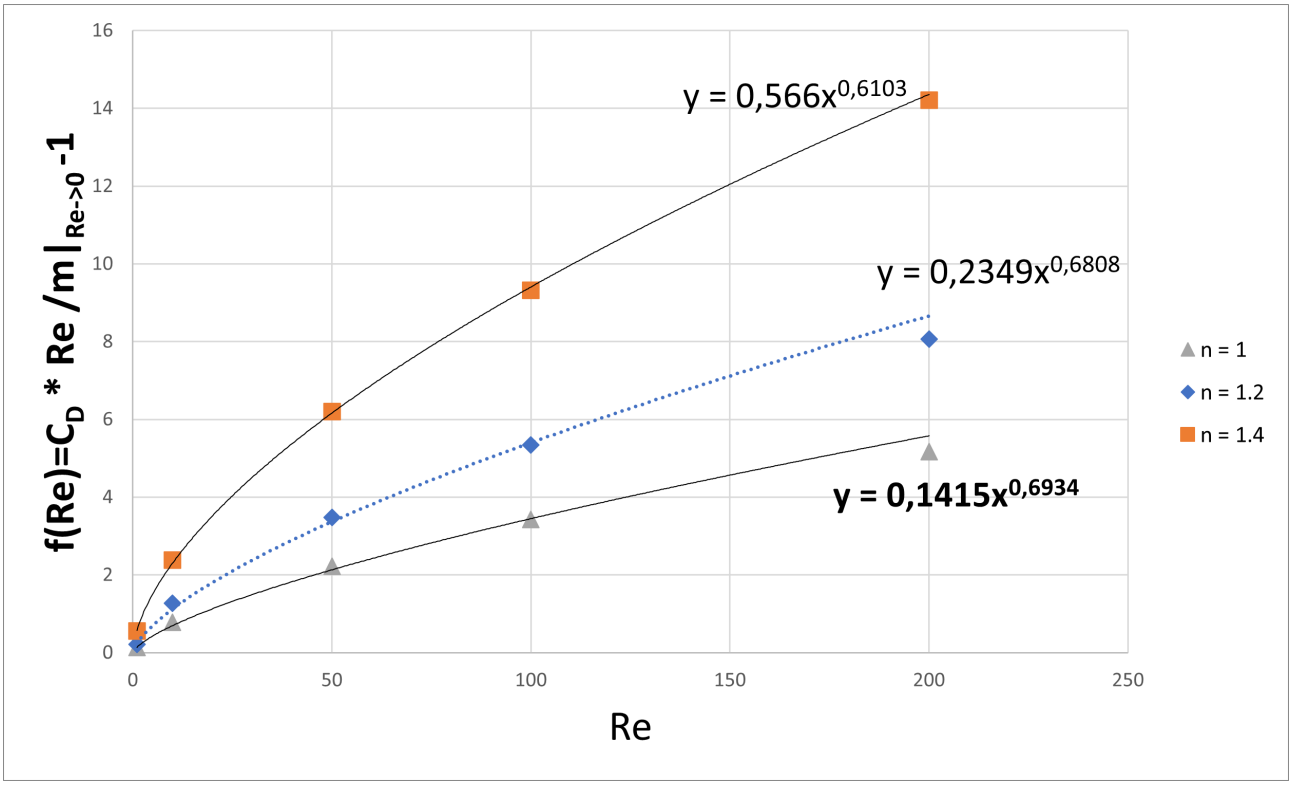

Figure 4: curve fitting of the $f(Re)$ from the C_D values for spheres in dilatant fluids. Curves are fitted for different n values: 1 (Newtonian case), 1.2, and 1.4. Raw data from: Tripathi et al. (2006)

$n = 1.4$ can be derived:

$$n = 1.2: \qquad C_D = \frac{19.85}{Re}(1 + 0.23Re^{0.681}) \tag{159}$$

$$n = 1.4: \qquad C_D = \frac{13.67}{Re}(1 + 0.57Re^{0.610}) \tag{160}$$

For all the cases in between, interpolation of the raw data can be made.

3 Numerical Procedure

A spectral scheme based on the Chebyshev polynomials is used for spatial discretization, whereas second-order backward differentiation is employed for the time derivatives.

3.1 Newtonian solver

The Newtonian case with the analytical solution found in Chapter 2.1.4 is first implemented into the code and then the Power law is adapted as well. The initial condition is taken as:

$$h = h_0 + r^2 \tag{161}$$

where h_0 is a constant that shows the minimum initial thickness of the film.

The dimensionless equations are implemented in MATLAB together with the boundary and initial conditions and solved numerically by use of a spectral method based on Chebyshev polynomials (Guo et al. (2013)).

The equations to solve are the kinematic condition Eq. 97, solving for the thin film thickness, and the stress balance, Eq. 77, solving for the pressure. The equations are discretized as:

$$\left[\frac{3}{2\Delta t}\mathtt{I}\right] h_{k+1} - \frac{h_k}{\Delta t} + \frac{h_{k-1}}{2\Delta t} = \left[diag\left(\frac{1}{12r}\right)[D]diag(h_k^3)diag(r)[D]\right] P_{k+1} \tag{162}$$

$$[\mathtt{I}]P_{k+1} = 2 - \left[diag\left(\frac{1}{12r}\right)[D]diag(r)[D]\right] h_{k+1} + \frac{A^*}{h_k^3} \tag{163}$$

At this stage, the tilde notation is omitted because it is clear that all equations are in dimensionless form. Here, k is the time step number, and the equations are solved at step $k+1$, therefore all terms which include $k+1$ are unknown. Terms including k or $k-1$ are known from solutions at previous time steps. Note that the square brackets indicate matrices of size $(N+1)\times(N+1)$, where N is the number of grids, and $N+1$ is the number of grid points, while the variables outside the square brackets, r, h_i, P_i, are column arrays of length $N+1$. $\mathtt{I}$ is the identity matrix, a square matrix in which each of the elements of its principal diagonal is a 1 and each of the other elements is a 0. Here it is represented of order $(N+1)\times(N+1)$. Moreover, Δt is the time step size. $[D]$ is the $(N+1)\times(N+1)$ derivative matrix, which is obtained through Chebyshev polynomials that are mapped linearly to fit the domain of $r=0$ to $r=r_\infty$. Here, r_∞ is a large enough distance from the collision zone, such that the collision doesn't affect the local conditions anymore. At each grid point, the matrix $[D]$ derives with respect to r. The *diag* operation also represents arrays that have been transformed into diagonal matrices. The two examples below, which each include an unknown array (f), are provided to demonstrate the need of this diagonalization:

$$[D]rf = \frac{\partial r}{\partial r}f, \tag{164}$$

The unknown array in this case is not subject to the derivative operator. Conversely, the results of the diagonalization are as follows:

$$[D][diag(r)]f = \frac{\partial}{\partial r}(rf), \tag{165}$$

the derivatives similar to that appear in both equations. The radial array and the unknown array, f, are both subject to the derivative operator in this case. The *diag* command in MATLAB carries out the following operation:

$$diag(r) = \begin{bmatrix} r_{(1)} & 0 & \cdots & 0 \\ 0 & r_{(2)} & \cdots & 0 \\ 0 & 0 & \cdots & r_{(N+1)} \end{bmatrix} \tag{166}$$

Gathering the unknown terms in the matrix equations, Eqs. 162 and 163, on the left-hand-side and combining them into a single matrix, yields:

$$AU = RHS \tag{167}$$

where U is a column array consisting of the unknown terms ($N+1$ nodal values of each h_{k+1} and P_{k+1}). The weights for the matrix A are defined by the discretized pressure and thinning equations. RHS is a column array that includes the known values. The matrix A is then further partitioned into four blocks, with one block representing each unknown variable in each equation, and they are written as:

$$\begin{bmatrix} A11 & A12 \\ A21 & A22 \end{bmatrix} \begin{bmatrix} P_{k+1} \\ h_{k+1} \end{bmatrix} = \begin{bmatrix} RHS1 \\ RHS2 \end{bmatrix} \tag{168}$$

The rows of the A blocks represent the thinning equation and pressure equation, while the columns represent the film thickness and the excess pressure, respectively. A is then of size $2(N+1) \times 2(N+1)$, while the right-hand side array and the array of unknowns are of length $2(N+1)$.

The weights shown below, which correspond to the unknown pressure and film thickness, are provided via the discretized thinning equation:

$$[A11] = \left[diag\left(\frac{1}{12r}\right)[D] diag(h_k^3) diag(r)[D] \right] \tag{169}$$

$$[A12] = \frac{\mathtt{I}}{\Delta t} \tag{170}$$

Then, the weights of the unknown terms in the pressure equation can be divided into the following blocks:

$$[A21] = \mathtt{I} \tag{171}$$

$$[A22] = \left[diag\left(\frac{1}{2r}\right)[D] diag(r)[D] \right] \tag{172}$$

The discretized thinning and pressure equations are then written with the following right-hand sides:

$$RHS1 = -\frac{h_k}{\Delta t} \tag{173}$$

$$RHS2 = 2 + \frac{A^*}{h_k^3} \tag{174}$$

Additionally, the boundary conditions must be included in the matrix A as well as on the right side of the related matrix equation. Boundary conditions for this set of equations are:

$$\text{for} \quad r = 0: \qquad \frac{\partial h}{\partial r} = 0; \quad \frac{\partial P}{\partial r} = 0 \tag{175}$$

$$\text{for} \quad r = r_\infty: \qquad \frac{\partial h}{\partial t} = -V_{app}(t); \quad P = 0 \tag{176}$$

where V_{app} corresponds to the approach velocity of the two bubbles. The approach velocity condition turns into:

$$h_{k+1} = -V_{app} * \Delta t + h_k \tag{177}$$

The boundary condition $\frac{\partial h}{\partial r}|_{r=0} = 0$ gives:

$$A_{(1,i)} = [D_{(1,i)} \quad 0 \quad 0 \quad \cdots \quad 0] \tag{178}$$

Note that the index i is the same as number of grid points $(N+1)$. The first row of the derivative matrix, D, is therefore filled in row 1 of A, column 1 to $N+1$. The remaining characters in row 1 are $(N+1)$ zeros. The second block multiplies the unknown pressures in the problem and while implementing a boundary condition on the film thickness the corresponding values in that block should be zero and vice versa. The corresponding right-hand side yields:

$$RHS_{(1)} = 0 \tag{179}$$

The boundary condition $\frac{\partial h}{\partial r}|_{r=r_\infty} = 0$ can be be implemented as:

$$A_{(N+1,i)} = [0 \quad 0 \quad \cdots \quad 1 \quad 0 \quad 0 \quad \cdots] \tag{180}$$

Here, the column $N+1$ of matrix A's row $N+1$ has a 1 that, in the thinning equation's point r_∞, corresponds to the variable h. This row's remaining spaces are all zeros. Following the time discretization employed in the thinning equation gives the following right-hand side entry in the position $N+1$:

$$RHS_{(N+1)} = -\frac{V_{app}}{\Delta t} + h_{k,(N+1)} \tag{181}$$

The boundary condition $\frac{\partial P}{\partial r}|_{r=0} = 0$ is expressed in A as:

$$A_{(N+2,i)} = [0 \quad 0 \quad \cdots \quad 0 \quad D_{(1,i)}] \tag{182}$$

which indicates that row $N+2$ in A is filled with the first row of the derivative matrix in column positions $N+2$ to $2(N+1)$, while the remaining space on the row is filled with zeros. The corresponding right-hand-side is expressed as:

$$RHS_{(N+2)} = 0 \tag{183}$$

Finally, the boundary condition $P|_{r=r_\infty} = 0$ gives:

$$A_{2(N+1),i} = [0 \quad 0 \quad \cdots \quad 0 \quad 0 \quad 1] \tag{184}$$

where row $2(N+1)$ of matrix A has entry 1 in column $2(N+1)$. The right-hand-side gives:

$$RHS_{(2(N+1))} = 0 \tag{185}$$

3.2 Non-Newtonian case solver

For the non-Newtonian case, the spectral method implemented is the same but the equations and the matrices are changed to follow the equation derived in Chapter 2.2.

Equations 139 and 140 are discretized in the following form:

$$\left[\frac{3}{2\Delta t}\mathtt{I}\right] h_{k+1} - \frac{h_k}{\Delta t} + \frac{h_{k-1}}{2\Delta t} = -\frac{n}{(1+2n)2^{1/n+1}} \left[diag(1/r)\right] [D] \left[diag(r)\right] \left([-D]\,[P_k]\right)^{1/n-1} \left[h_k^{2n+1}\right] [-D]\, P_{k+1} \tag{186}$$

$$[\mathtt{I}]\, P_{k+1} = 2 - \frac{1}{2} \left[diag(1/r)\right] [D] \left[diag(r)\right] [D]\, h_{k+1} + \frac{A^*}{h_k^3} \tag{187}$$

and solved simultaneously with the boundary conditions presented in Eqs. 175 and 176.

3.3 Implementation of force balance and search algorithm

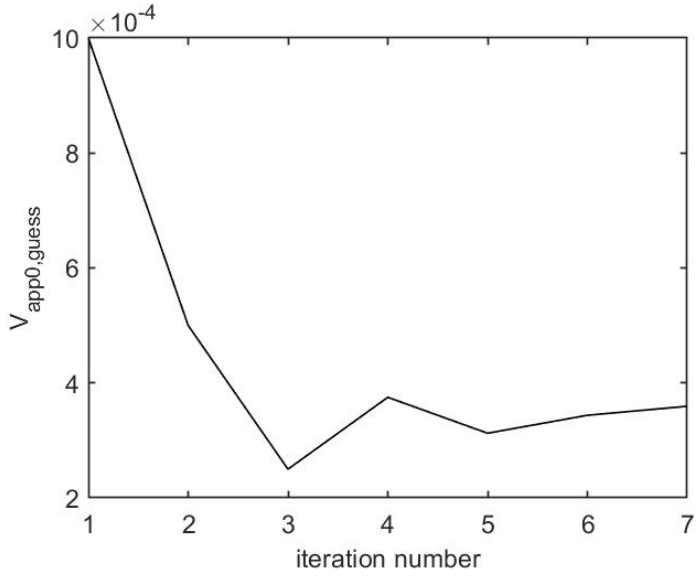

Figure 5: Evolution of $V_{app0,guess}$ with search iterations until convergence to V_c along the iteration steps.

The default values of the simulation parameters are estimated based on air-in-water particles. Fluid particles of 1 mm are considered. The added mass coefficient value of air as the dispersed phase is $C_m = 0.803$ (Kamp et al. (2001)). This coefficient is of usage for the calculation of the default values of m_A and Oh_A. The particle velocities V_1 and V_2 are calculated via Eq. 149 to give $V_{app}(t)$ and solved in an external function. This is coupled and solved simultaneously with the main set of equations derived before Eq. 139 and Eq. 140. Eq. 149 is an ordinary differential equation and its discretized form is the following:

$$v_{k+1,i} = \left(a(1-\rho_c/\rho_d)g - (-1)2\pi \cdot \left[\int_0^{r_\infty} rP\,dr\right] Oha2 - Oha_2 \cdot b \cdot v_{k,i} + \frac{v_{k,i}}{\Delta t}\right) / \frac{1}{\Delta t} \tag{188}$$

where v_{k+1} is the particle velocity and v_k the particle velocity at the previous iterative step. Both are column arrays of length $N+1$ and $i = 1, 2$, identifying the two different particles. ρ_c and ρ_d are the density of water and air, respectively of the continuous and dispersed phases. The parameters a and b contain within them the values of the other multiplicative constants present in Eq. 149. P here is a matrix containing all the values of pressure P_{k+1} obtained from the Non-Newtonian solver. In order to carry out the integration, the built-in function of MATLAB *trapz* is used which integrates the pressure function with respect to the coordinates or scalar spacing specified by r.

In order to find the critical approach velocity, a small optimization algorithm has been implemented for fast convergence of the solver. After selecting an initial approach velocity $V_{app0,guess}$, the solver would increase or decrease this value at the end of every simulation round based on whether the outcome was coalescence or rebound, and then start another simulation with this new value of the approach velocity. If the outcome is rebound, it is stored in a matrix called $V_{app0,max}$, while if it is coalescence, it is stored in a matrix called $V_{app0,min}$. Storing all the values from the previous iterations is important in order to set boundaries that cannot be exceeded. For example, if in an iteration the outcome is rebound, this is stored into the $V_{app0,max}$. If the

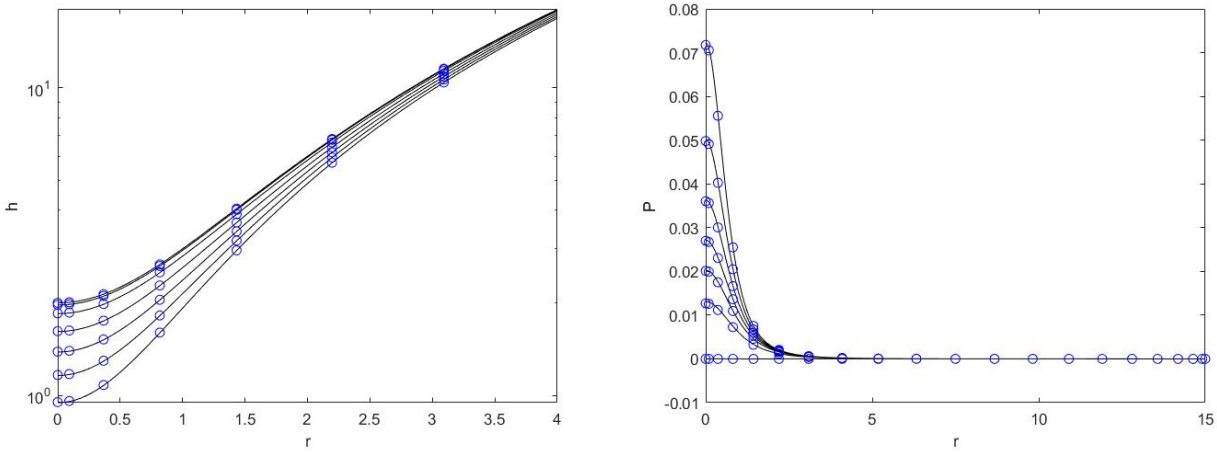

(a) Film thickness as a function of r and t.

(b) Pressure as a function of r and t.

Figure 6: Pressure and Film Thickness. The model parameters are: $V_{app} = 0.05$, $A^* = 0.0001$, time steps $dt = 0.01$. The simulation result is marked by circles and the black curve shows the reference from Fanebust et al. (2021)

following outcome is coalescence, these values would be increased for the following third iteration but compared with the smallest value stored inside the matrix $V_{app0,max}$. Doing so, at the end of each loop the velocity was changed but kept within the boundaries set by the values obtained from the previous iterations. And so on, until the value converges to the critical approach velocity V_c. In this way, a fully-automatic and efficient search algorithm is implemented which achieves faster convergence, and no extra work is done by iterating for values for which the outcome was certainly already known. An example for the typical progression of $V_{app0,guess}$ during search iterations is shown in Fig. 5.

4 Results and Discussion

The drainage model employed in this work allows the particle velocities, and as a result, V_{app}, to change throughout the drainage process by integrating a force balance for each particle in the model. Moreover, the results presented in this work are not limited to the interactions between two bubbles but cover droplet-droplet interactions as well. This is because the default values of m_A and Oh_A are calculated based on the air bubbles but the parameter values calculated for a typical droplet of the same size, are on the same order of magnitude as the estimations for the bubbles. Furthermore, the model is the same for both droplets and bubbles.

The following chapter starts with the validation of the codes used in this thesis, and then attention will be given to how the solver works and how rebound and coalescence were investigated with it. Then, the effects of the major key parameters affecting the values of the V_{app} are discussed: the analysis starts evaluating how the solution changes with a power law type drag force compared with a Newtonian continuous media, and then the effects of the different parameters contained inside the power law are analyzed.

4.1 Validation

The validation of the code is done in two phases: first the validation of the implementation of the non-Newtonian drainage equations and then the validation of the force balance applied on the moving particles.

4.1.1 Validation of the Non-newtonian code

The results of the research work can be now validated with the results of previous similar work, in this case the one carried out by Fanebust et al. (2021). Fig. 6 shows how the two solvers give the same outcome for film thickness and pressure in the same range of r.

4.1.2 Validation of the Force balance

In order to validate the addition of the force balance to model the approach velocity, studies carried out by Ozan et al. (2021) were used. Here, V_c, the critical velocity explained in Chapter 2.3.1, is presented as a function of the equivalent particle radius, R_p for immobilized air-in-water particles, which is a common occurrence in many real systems. The curve fit on the V_c data from this study is plotted in Fig. 7 together with the results

from the data model calculated in Eq. 149. The typical critical velocity values presented here range between 2×10^{-4} and 3×10^{-3}, which corresponds to 1.45 cm/s and 21.8 cm/s when the velocity scale is calculated for air in water systems. Both plots are made for the dimensionless value of the critical velocity against R_p. A qualitative comparison on the V_c model is possible. For smaller particles the current model agrees with the

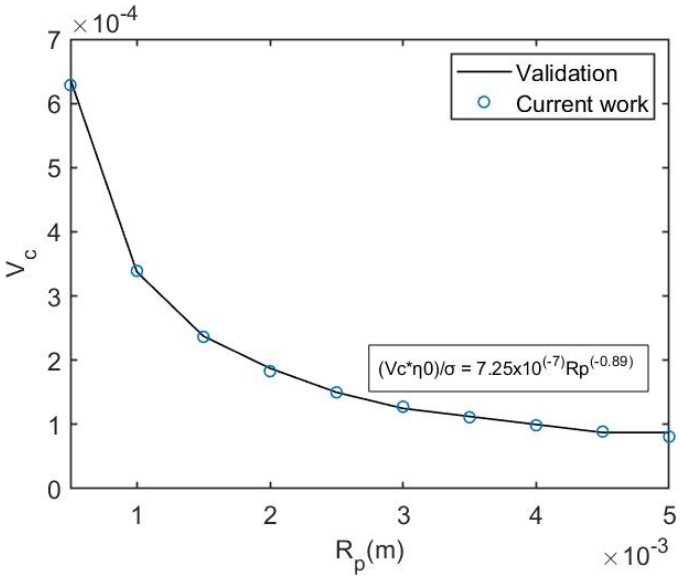

Figure 7: Effect of particle radius on V_c in a Newtonian system. The simulation result is marked by circles and the black curve shows a fit based on the reference adapted from Ozan et al. (2023)

ones estimated by Duineveld (1998) and Ribeiro and Mewes (2007)'s experiments. For larger particles, on the other hand, the model still estimates a decrease in V_c as the particle size increases, however, the decrease in the predicted V_c values seems to diminish as the particle size increases further, which may resemble the constant V_c behavior observed in the experiments of Lehr et al. (2002), and Ribeiro and Mewes (2007). Finally, the current work shows that V_c for the current model fits with high accuracy the model from Ozan et al. (2021) and Ozan et al.(2023), where V_c was estimated as $\propto R_p^{-0.9}$.

4.2 Rebound and Coalescence

The integration of the force balance to render the time-dependent behavior of V_{app} allows the film drainage model to capture not just the coalescence outcome (like in previous works using constant approach velocity collision by Ozan and Jackobsen (2019a), but the rebound outcome is also possible. Fig. 8 shows the behavior of the film for a collision with rebound outcome. In Fig. 8(a) the film thickness gets thinner as the time steps increase as the particles get closer. It should be noted that there is a difference from previous similar works: from Ozan et al. (2021) the film thickness gets thinner and interfaces are allowed to deform following the typical dimple shape, and the deformed radius increases but here, no tangential mobility undergoes. Figure 8(c) reveals that the particles slow down during the approach, since kinetic energy is depleted by the drag forces acting on the particles but no kinetic energy is converted to surface energy since interfacial deformations are not allowed. As shown in Fig. 8(d), the magnitude of the total film force acting on the particles increases during the approach, especially at the moment when particles collide, dropping down significantly immediately after. This reversal indicates the beginning of the rebound process, and the film force starts to decrease due to reducing pressure build-up in the film, while the energy stored at the surface starts being converted back to kinetic energy. After the collision, the film force passes through a maximum and afterwards asymptotically approaches zero indicating that the spherical particle shape at the beginning of the interaction is recovered. The changes in V_{app} in the latest stage of the interaction are due to the drag force only.

Coalescence mechanisms describe the process of particles merging into one another to form a bigger one. When the attractive intermolecular forces are included, the film drainage model is able to estimate the coalescence outcome, as mentioned above. The coalescence mechanism is identified by the coalescence of two closely spaced particles and, since the film drainage model is not capable of rendering the film rupture, is assumed that this is achieved when a sufficiently small thickness is reached, because the film begins to thin rapidly due to the attractive Van der Waals forces. However in this work, due to the assumption of no tangential mobility, a proper coalescence can't be observed. The film force creates huge resistances that are too high to be broken since no kinetic energy is converted into surface energy because no interfacial deformations are happening. It is a balance between the film force and the Hamaker constant whether rebound or coalescence happens and

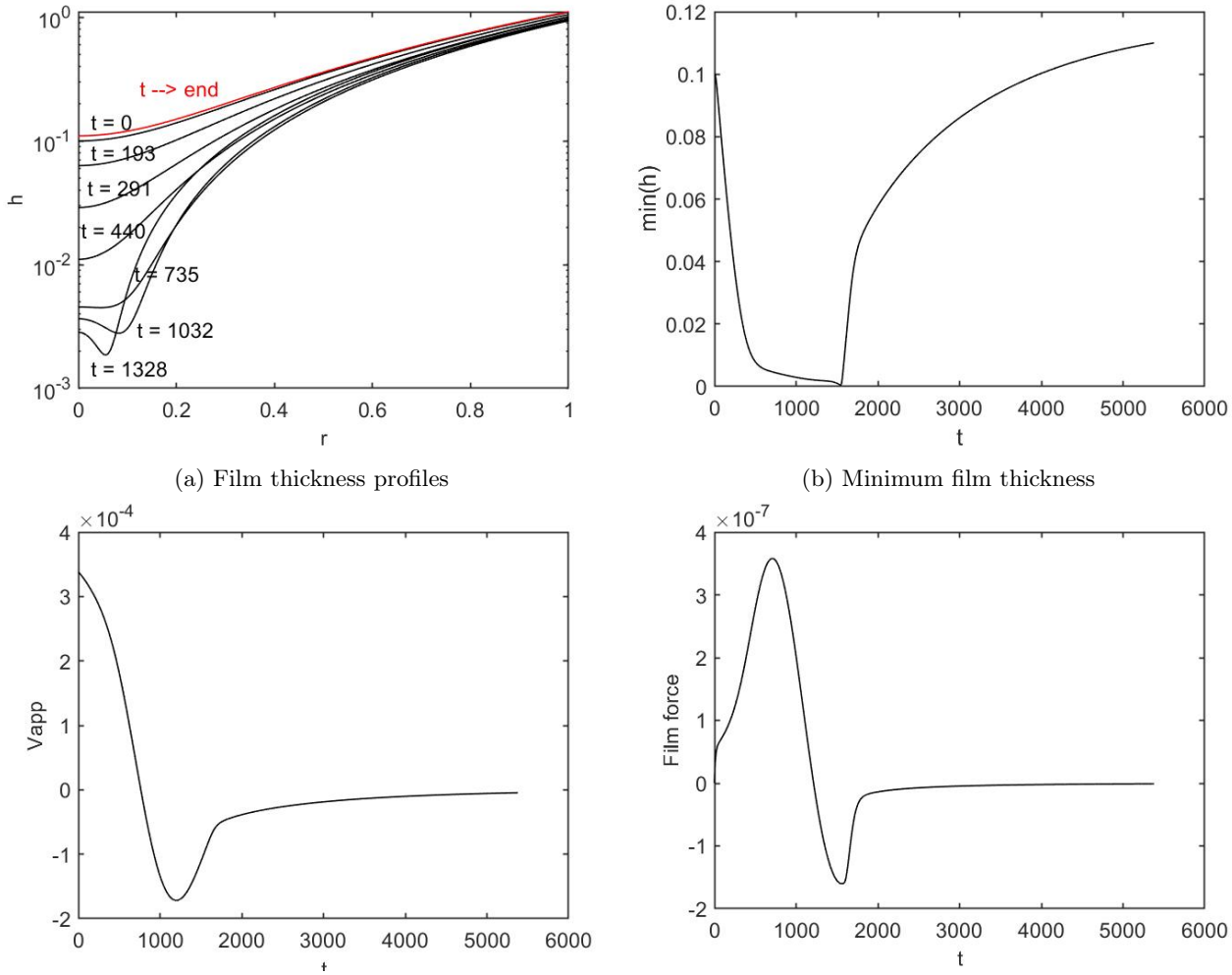

(a) Film thickness profiles

(b) Minimum film thickness

(c) Approach velocity

(d) Film force

Figure 8: A collision with rebound outcome: (a) film thickness profiles, (b) minimum film thickness, (c) the approach velocity, and (d) the total film force acting on the particles as functions of time. The model parameters are $Rp = 0.001$, $V_{app,0} = 1 \times 10^{-4}$, $V_{2,0} = -V_{1,0} = V_{app,0}/2$, $h_{min,0} = 0.1$, $Oh_A^2 = 8.2 \times 10^{-6}$, $A^* = 10^{-13}$ and $n = 0.95$.

in order to achieve coalescence with the assumption of immobile interfaces, the Hamaker constant and the value of A^* should increase a lot to overcome the film force. But such values would be unrealistic to get the indication of the film rupture when the interface is immobile. However, in Ozan and Jakobsen (2019a) the model is actually capable of estimating coalescence when the interfaces are not immobile. Another way to push the coalescence would be of increasing the radius of the particle, in order to increase the Oh_A number and consecutively increment the drag force. On the other hand, increasing the radius of the particle would give fake coalescence results, like it is shown in Fig. 9. It is clear that coalescence is not happening interior of the domain but on the boundary, not in accordance with the model assumption. Due to the assumption of gentle collision, the coalescence should happen close to the center of the domain. This behavior is the result of the implementation of the boundary conditions and not because of the application of the film drainage model itself. This is not a physical outcome and it is predominantly seen for larger radii. Yet, coalescence can be identified in the simulation by the steady-state outcome as shown in Fig. 10. The steady-state is a low-energy collision in which the particles after bouncing reach a halt at a minimum thickness smaller than $h_{min,0}$, as their kinetic energy is depleted before the film gets thin enough for coalescence and resistant enough for particles to rebound. This outcome is neither a coalescence nor a rebound but it represents the beginning of the interaction between the particles, a transitional middle stage connecting coalescence and rebound outcomes. Despite the limitations of the simulation, in a real system, with stirrings and currents, it is likely that if a perturbation or a secondary mechanism that supplied kinetic energy to the particles would occur in the system, the steady-state would be disturbed and the collision would result in coalescence. In this work, this type of steady-state will always be treated as a proper coalescence, assuming disturbances would later turn into coalescence. Figure 10(c) shows the two particles' approach and, simultaneously Fig. 10(b) shows that the film between them gets thinner before

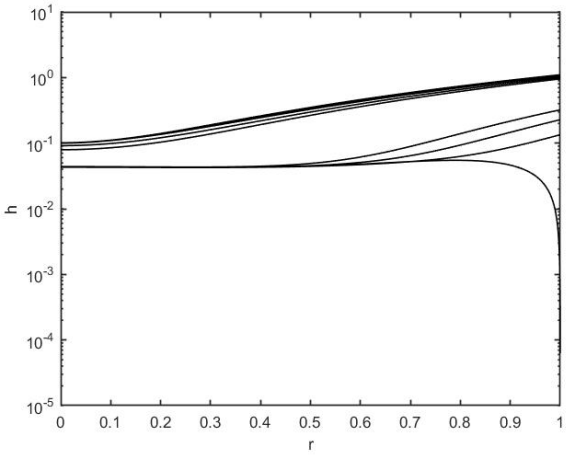

Figure 9: Non-physical coalescence outcome. Film thickness profiles during particles approach. The model parameters are $Rp = 0.001$, $V_{app,0} = 1 \times 10^{-4}$, $V_{2,0} = -V_{1,0} = V_{app,0}/2$, $h_{min,0} = 0.1$, $Oh_A^2 = 8.2 \times 10^{-6}$, $A^* = 10^{-13}$ and $n = 0.95$.

they start departing from each other until there is no more energy to push them apart enough to rebound and the approach velocity becomes zero, and the minimum film thickness reaches also a steady height.

4.3 Force Balance

4.3.1 Newtonian continuous media vs Power law type drag force

It is important to analyze and sum up the effect of using a power law type of drag force within the force balance. As can be seen from the following figures, Fig. 11(a), and Fig. 11(b) the change is extremely minimal, both as regards the use of the Eq. 157 for thinning fluids, and for the use of the Eqs. 159 and 160 for thickening fluids. Such plots are made by comparing the h_{min} for different n at the same initial approach velocity: at such velocity ($V_{app0} = 0.0003$) the outcome is for the most of n steady-state, expect for $n = 0.90$ with Newtonian drag force expression which is coalescence. Both plots show that using a drag force closure model to model the non-Newtonian behavior of the continuous phase does not really affect the final results. Both graphs show that while the behavior of the minimum film thickness is not influenced by the drag force expression used at all, the power law parameters are very significant inside the solutions of the governing and interfacial equations. Even though the flow around a sphere depends on the viscosity of the fluid the matter flows in, fluids with Newtonian and power-law drag forces have similar flow patterns. As can be seen in Fig.12, the power-law drag force does not really affect the plot of the critical velocity as well.

This not altogether unexpected result could agree with the fact that the drag force is of little significance in contexts in which very small distances and particles are considered and takes second place to, for example, the film force. This is because the force balance is an external and additional element to the problem. However, the type of non-Newtonian fluid used is of greater value as regards its impact on the axial component of the momentum equation: this is because the momentum balance is a governing equation and inside of it the viscosity is of great importance and a change of the expression used to define it is much more impactful on the final solution of the problem.

This was verified for slow scenarios in the ranges of radii and velocity of importance as well as for values of n not too distant from the Newtonian case. Since the addition of the power law drag force in the force balance does not really affect the results, the effects of the other parameters on the model will be analyzed only for the general Newtonian type of force balance, for an easier understanding of the results.

4.4 Effects of Power law parameters

4.4.1 Effect of the flow behavior index, n

Figure 13(a) shows the time development of the h_{min} for varying values of the power index, n, for shear thinning fluids, $n < 1$, while 13(b) shows the time development of the h_{min} for shear thickening fluids, $n > 1$. The plots are both made at the same initial approach velocity V_{app0} and at the same particle radius. At this initial velocity, in the Newtonian case, to use as a reference in order to compare the other n values, the particles will not bounce but, instead, steady-state is the outcome. As the n value changes, the outcome varies between steady-state and coalescence.

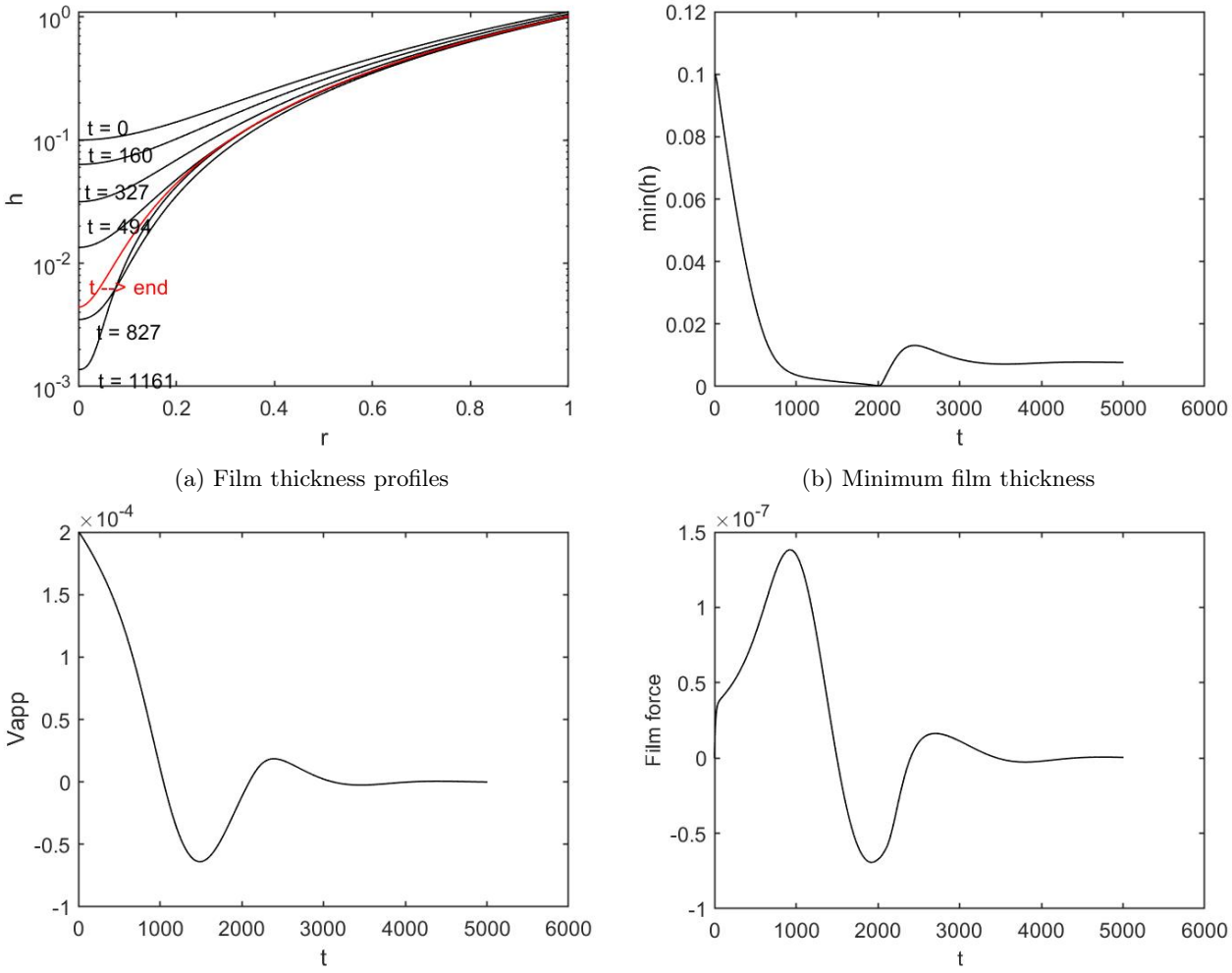

(a) Film thickness profiles

(b) Minimum film thickness

(c) Approach velocity

(d) Film force

Figure 10: A collision with steady-state outcome: (a) film thickness profiles, (b) minimum film thickness, (c) the approach velocity, and (d) the total film force acting on the particles as functions of time. The model parameters are $Rp = 0.001$, $V_{app,0} = 1 \times 10^{-4}$, $V_{2,0} = -V_{1,0} = V_{app,0}/2$, $h_{min,0} = 0.1$, $Oh_A^2 = 8.2 \times 10^{-6}$, $A^* = 10^{-13}$ and $n = 0.95$.

For n values not so far from the unity, the behavior is almost identical to the Newtonian one. For shear thinning fluids, when the value of n starts decreasing, the approach of the two bubbles is faster and they stay for a shorter time in contact before the bounce happens. For $n = 0.95$, there is a small bounce back but then the particles don't have enough energy to bounce to the initial position and a steady-state mechanism is shown in the graph, exactly as for the Newtonian case. As the n decreases, this small bouncing disappears and the particles just come together, showing coalescence. For shear thickening fluids, as the values of the n increase, the particles find a harder time to get that close as shown in Fig. 13(b).

Figure 14 present the time development of the film thickness profiles for varying values of the power index, n, for both shear-thinning and shear-thickening fluids. Here, all show rebound outcomes. Furthermore, the profiles look very similar but shifted upwards, meaning that the liquid gets harder to drain out completely as the fluid becomes more shear thickening, blocking the particles to enter in contact. The last plot shows how the minimum thickness is almost three times larger than the one in the top right corner, showing how influential is the value of n to the behavior of the drainage.

The more shear-thinning the continuous phase, the easier the film drainage, meaning the coalescence gets easier as the value of the power-law exponent decreases. This is expected as shear thinning fluids get less viscous as a stronger force is applied to them: the approach of the two particles increases the film force between them, decreasing the viscosity and making the drainage of the liquid of the part of the liquid in between the particles easier. Supposedly, the trend should be the opposite for shear thickening fluids: as a stronger pressure is applied on the thin film, the viscosity should increase, making the drainage slower or harder to achieve. This could be the reason why in Fig. 13(b), as the n value increases, the particles can't keep their interfaces as close up. At the same initial approach velocity, with the increasing shear thickening behavior, the fluid becomes more

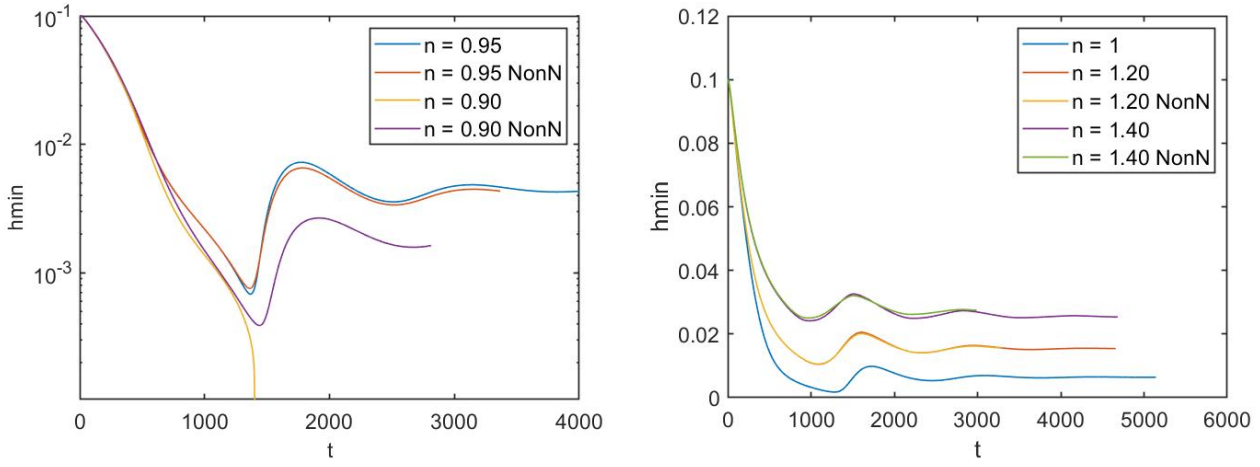

(a) Different shear thinning fluids.

(b) Different shear thickening fluids

Figure 11: Comparison of the h_{min} for Newtonian and power law drag force expressions at the same approach velocity $V_{app} = 0.0003$, and $Rp = 0.0005$.

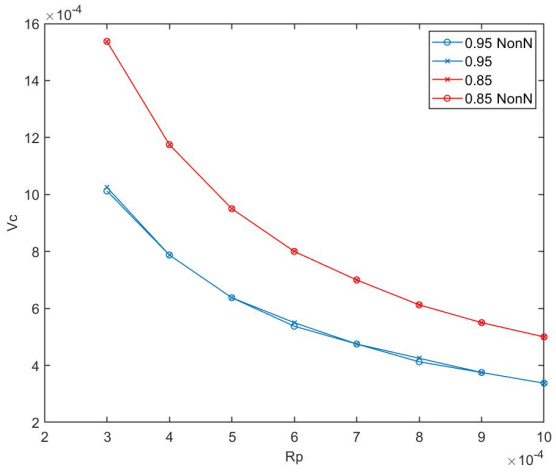

Figure 12: Comparison of the effect of the Newtonian and the non-Newtonian drag force expressions of an unbounded fluid in a power-law fluid on the critical velocity

viscous and drains out less because more friction is applied. For shear thickening fluids, when the minimum film thickness starts increasing for the first time is almost identical to for shear thinning, Fig. 13(a) and (b), but the graph is shifted upper and upper as the n value increases. Although the particles are less likely to get too close, even though after bouncing they all don't have enough energy to rebound, and steady-state happens in each case. In Fig. 14, not big differences can be seen.

For a better comparison of shear thinning and shear thickening fluids, the plots of the dimensional critical velocity can be compared. It is important to compare the critical velocity for different n values using its form with dimension since the velocity scale itself actually depends on the power law parameters. The critical relative approach velocity calculated in the simulation is a dimensionless value from Eq. 149. By converting it into a dimensional value, it is possible to evaluate the effects of the key parameters of the power law: k, known as the flow consistency index, and n, known as the behavior index. For definition:

$$V_c(m/s) = \tilde{V}_c \bar{V}_c \tag{189}$$

Since the scale of the velocity is $\bar{V} = \frac{\sigma}{\eta_0}$:

$$V_c(m/s) = \tilde{V}_c \frac{\sigma}{\eta_0} \tag{190}$$

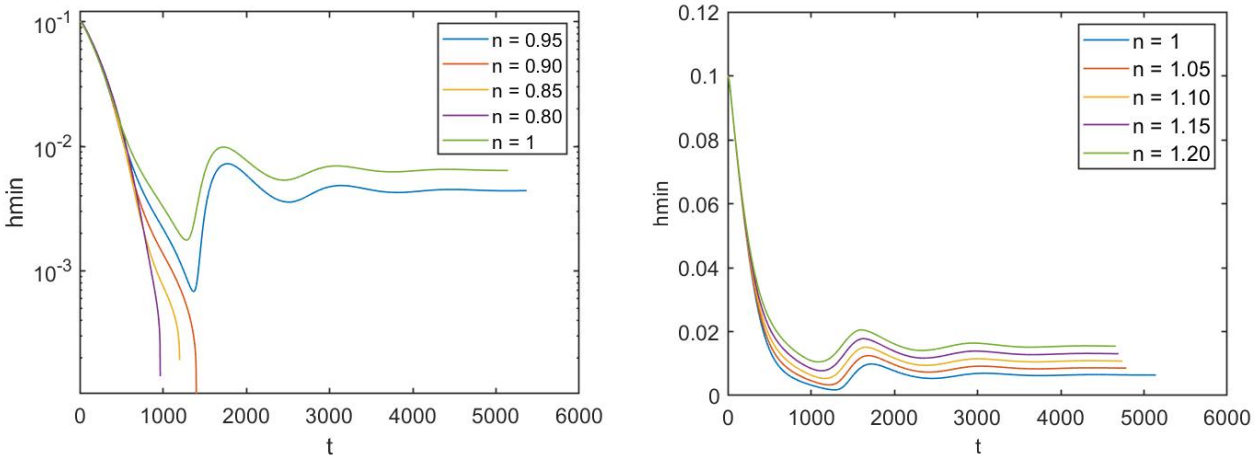

(a) Shear thinning fluids

(b) Shear thickening fluids

Figure 13: Time evolution of the minimum film thickness for different n: initial approach velocity $V_{app0} = 0.0003$ and $Rp = 0.0005$. Most of the cases at this initial approach velocity show steady-state outcome. On the left, three cases, for $n < 1$, show coalescence. The plot on the left is on logarithmic scale for the $y-$axis.

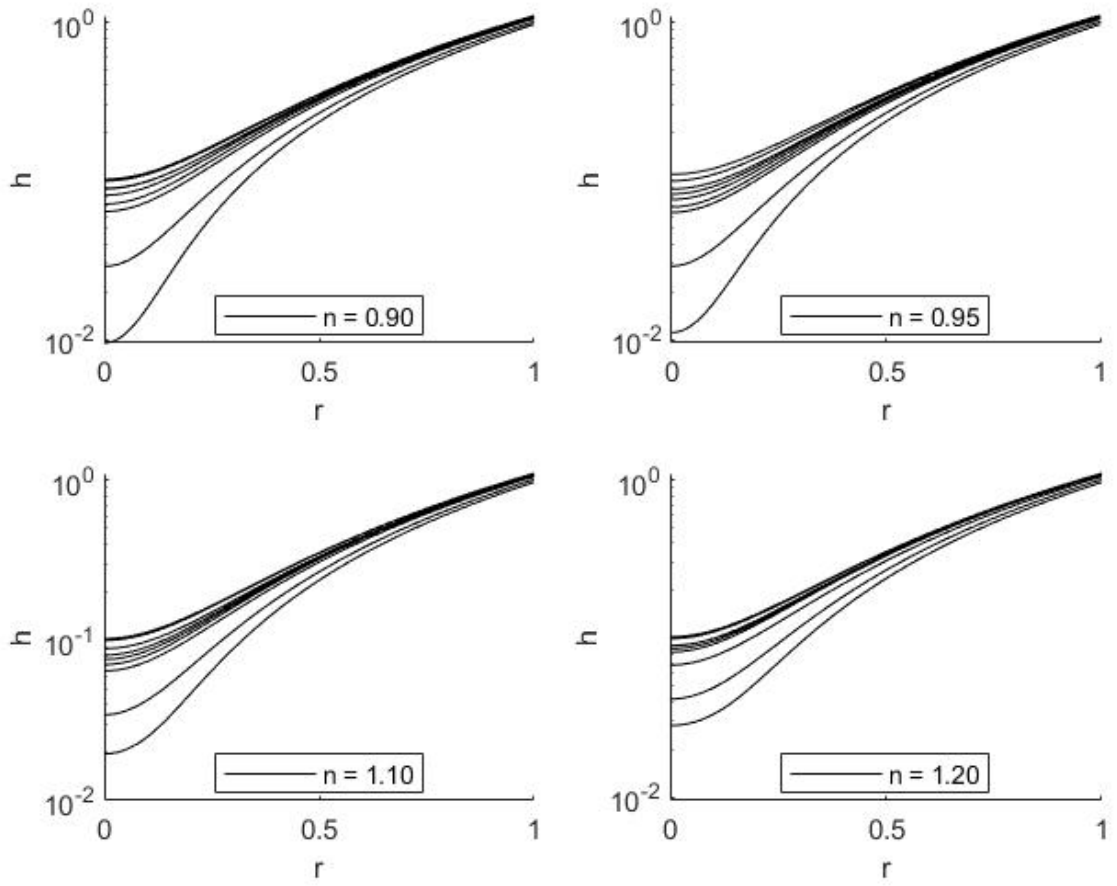

Figure 14: Time evolution of the film thickness for shear-thinning fluids ($n < 1$) and shear-thickening fluids ($n > 1$), $Rp = 0.001$

The scale of the viscosity is $\eta_0 = m\left(\frac{\bar{V}}{R_p}\right)^{n-1}$ and can be solved for η_0 by inserting the scale of the velocity:

$$\eta_0 = k\left(\frac{\frac{\sigma}{\eta_0}}{R_p}\right)^{n-1}$$
$$(\eta_0)^n = k\left(\frac{\sigma}{R_p}\right)^{n-1}$$
$$\eta_0 = k^{(1/n)}\left(\frac{\sigma}{R_p}\right)^{1-1/n} \tag{191}$$

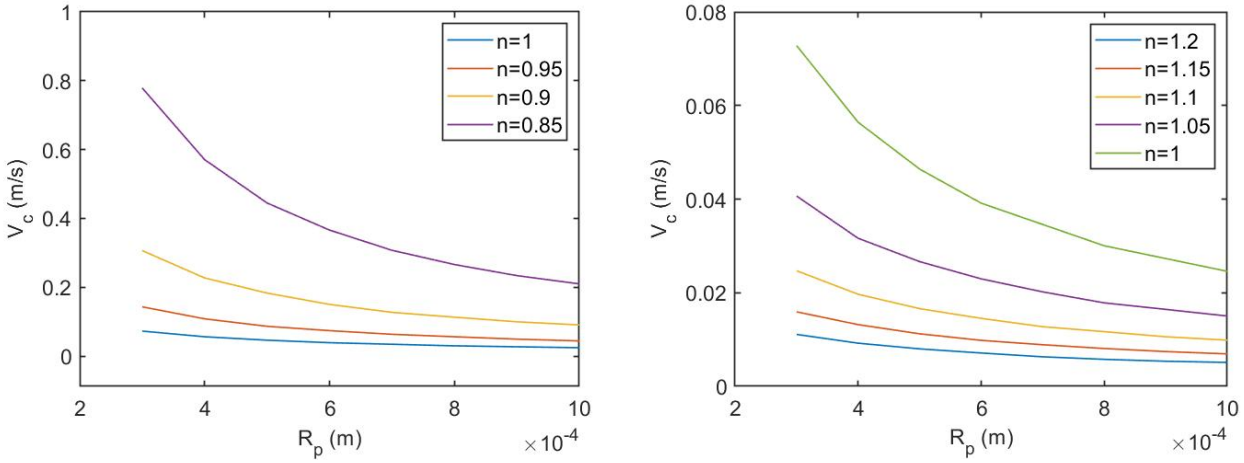

(a) Shear thinning fluids

(b) Shear thickening fluids

Figure 15: Effect of the power-law index on the critical velocity for different type of fluids.

The equation of the critical velocity with dimensions becomes then:

$$V_c(m/s) = \tilde{V}_c \frac{\sigma}{k^{(1/n)} \left(\frac{\sigma}{R_p}\right)^{1-1/n}} \tag{192}$$

Figures 15(a) and (b) show the trend of the critical velocity with the power-law index. As mentioned, with the increasing shear thinning behavior, $n < 1$, the drainage gets easier as the fluid becomes more viscous and drains out smoother. Supposedly, the trend should be the opposite for shear thickening fluids: as a stronger pressure is applied on the thin film, the viscosity should increase, making the drainage slower or harder to achieve. Then rebound would show up at lower values of velocity. Accordingly, the simulations show that the critical velocity for the smallest rebound possible is actually decreasing as the behavior of the fluid gets more shear thickening, while it increases for shear thinning fluids. This increase is much more emphasized for shear thinning than the decrease for shear thickening. Figure 15(a) shows how for shear thinning fluids the V_c increases much more than how shear thickening decreases on the other side in Fig. 15(b). The critical velocity does not escalate as strongly for shear thickening fluids. Since shear thickening films make coalescence harder to achieve, the critical velocity diminishes as the fluid becomes more shear thickening i.e., with increasing n. Since coalescence is easier to achieve when the film is shear thinning, the critical velocity for the first rebound has to rise to higher values. Again, for values of the power law exponent close to the unity the critical velocity is almost the same, and big changes are not visible. As the fluid becomes more shear thinning, rebound does become harder to achieve. For pseudoplastic fluids, When pressure or sudden force is applied to its viscosity is reduced, it becomes "thinner" and flows or pours more easily. As the pressure in the thin film increases due to the approaching particles, coalescence is favoured and in order to get rebound, higher velocities are needed. Meanwhile, rebound is facilitated by the increase in the shear thickening behavior. This may be in agreement with previous studies which confirm that coalescence is slower to obtain for dilatant fluids: in fact, the graph of the minimum thickness, Fig. 13, shows that as the index n increases, the particles find a harder time to enter in contact. It is reasonable to think that shear thickening fluids are harder to drain compared to shear thinning. As stress increases for such fluids, the viscosity increases and more force is required for the same amount of strain. The particles then rebound on such thin film more easily and smaller velocities are required to achieve this.

4.4.2 Effect of the flow consistency index, k

Again, the dimensional velocity is analyzed and plotted using Eq. 192. By using a range value for the flow consistency index k of [0.001 0.0015 0.002], close to the values of water's viscosity, it is possible to obtain a plot of the critical velocity against the equivalent particle size.

The parameter k influences the system actually in one way: it affects the final scale of the curves without interfering with the simulation itself. This parameter does not appear in the model directly, meaning that it does not show up in the dimensionless equations but its effects are observable only in the scales during the process of turning into dimensional values the V_c. The solution is then a single solution but it is possible to plot V_c in dimensional form using different values of k, as shown in Fig. 16 As the value of the flow consistency index increases, the curve is more and more shifted downwards, the value of the critical velocity decreases meaning

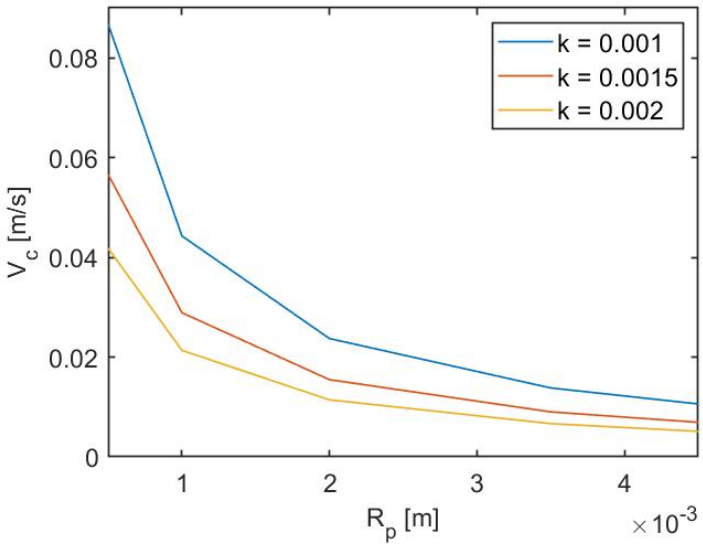

Figure 16: Effect of different flow consistency index on the critical velocity plot. The model parameters are V_cs from the simulation for Rp=0.0008 and n=0.95, $\sigma = 0.0728$

that film drainage is harder to achieve and rebound is favored. As k increases, the film gets more viscous, like for shear thickening fluids, because this term multiplies the viscosity directly and at the same time from Eq. 192 it diminishes the value of the critical velocity.

4.4.3 Challenges and future work

As the power-law index decreases, further investigations won't produce significant results. The plot of the critical velocity for n equal to 0.80 is not shown in Fig. 15(a) because after this n, the approach velocity must scale to very high values in order to counteract the viscosity of the liquid and obtain the rebound of the particles as a final result, around $4(m/s)$ and 2 (m/s). However, these speeds are absurdly high as to be unrealistic, not common at an industrial level, outside any common range in which they are normally studied. Moreover, the solver for values of n greater than 0.70 fails to converge: particles rebound even before getting closer, as shown in Fig. 17. The stronger shear thinning behavior reduces the possibility for the spheres to rebound and searching for the velocity that will give the first possible rebound outcome is not useful as the velocities would exceed real processes and industrial application values even more than for 0.80. One way to improve

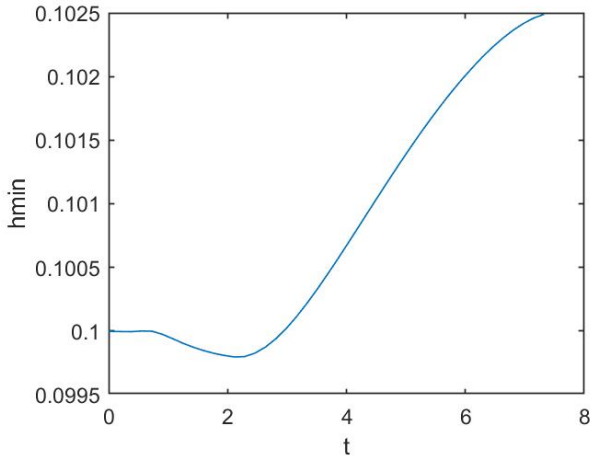

Figure 17: Plot of the h_{min} at the rebound of particles for $n = 0.70$ and $R_p = 0.0005$

and develop further this study in the future would be to find a solution that is more suitable and real for shear thinning fluids: maybe a power law type fails to represent in a plausible way the behavior of these fluids for n below $n = 0.80$ and a more suitable experimental law should perhaps be introduced instead for more realistic results. Another suggestion would be to change the initial film thickness $h_{min,0}$: perhaps starting from further distances could allow the system to interact better by enabling the particles to come into contact.

A possible future work to extend this study would be to represent drainage differently, perhaps by introducing tangential mobility into this model. This would increase the complexity of the system and the equation to solve, slowly removing limiting assumptions and simplifications for a more realistic representation of the problem instead of describing just immobile systems. Equations would become more elaborated and the numerical method for finding a solution more complex. This would be an interesting future challenge. Since the drag force at such a small molecular level counts for very little, perhaps going into more detail on how the forces are distributed at a surface and at a tangential level would be a more accurate representation.

5 Conclusions

The drainage of a thin non-Newtonian film entrapped between two fluid particles is examined in this thesis. The power law is used to calculate the non-Newtonian viscosity of the continuous phase, which is treated as a generalized Newtonian fluid. Although they are considered deformable, the interfaces cannot move tangentially. A force balance that accounts for the drag, film, and the added mass forces was applied to the system in order to construct a time-dependent approach velocity. This model is capable of both coalescence and rebound because of the addiction of this force balance. Different models drawn from experimental data, capable of representing the non-Newtonian behavior of the drag force within the force balance, were compared. From their application, the appreciable results have been few, signaling how a type of drag force that is of Newtonian type or of power law type has little influence at small particle level and such small speeds. The same cannot be said of the influence of the power index n on the viscosity of the continuous phase. Through it, the impact of non-Newtonian behavior on the film drainage and coalescence time is investigated. From the model, it can be seen that the non-Newtonian behavior is very influential on the coalescence time: as the fluid becomes more shear thinning, the drainage is facilitated and particles are more prone to coalesce. Furthermore, the flow consistency index effects, k, were analyzed. As this parameter increases, the film becomes more viscous, making drainage harder and promoting rebound. A critical initial approach velocity, for which the rebound is seen for the first time for a given parameter set is defined as Vc. Vc is decreased, and so rebound facilitated, by an increase in the radii of the particles and by an increase in the power index n, especially above the unity, since the fluid becomes more viscous and drains out less because more friction is applied to it. At the same particle size, coalescence starts to occur faster in shear-thinning fluid than in Newtonian fluid, and the critical velocity V_C rises a lot.

References

Abid, S., and A. K. Chesters. "The drainage and rupture of partially-mobile films between colliding drops at constant approach velocity." International journal of multiphase flow 20.3 (1994): 613-629.

Boyde, Steve. "Green lubricants. Environmental benefits and impacts of lubrication." Green Chemistry 4.4 (2002): 293-307.

Chesters, A, K. "Modelling of coalescence processes in fluid-liquid dispersions: a review of current understanding." Chemical engineering research and design 69.A4 (1991): 259-270.

Davis, Robert H., Jeffrey A. Schonberg, and John M. Rallison. "The lubrication force between two viscous drops." Physics of Fluids A: Fluid Dynamics 1.1 (1989): 77-81.

Dazhi, Gu, and R. I. Tanner. "The drag on a sphere in a power-law fluid." Journal of Non-Newtonian Fluid Mechanics 17.1 (1985): 1-12.

Derjaguin, B. V., and M. Kussakov. "Anomalous properties of thin polymolecular films." Acta Physicochim. URSS 10.1 (1939): 25-44.

Dhole, Sunil D., Raj P. Chhabra, and Vinayak Eswaran. "Flow of power-law fluids past a sphere at intermediate Reynolds numbers." Industrial & engineering chemistry research 45.13 (2006): 4773-4781.

Dudek, Marcin, et al. "Microfluidic method for determining drop-drop coalescence and contact times in flow." Colloids and Surfaces A: Physicochemical and Engineering Aspects 586 (2020): 124265.

Fanebust, Maria, Suat Canberk Ozan, and Hugo Atle Jakobsen. "Coalescence of fluid particles with deformable interfaces in non-Newtonian media." International Journal of Multiphase Flow 144 (2021): 103787.

Fanebust, Maria. "Investigation of coalescence through film drainage modeling in chemical-and bioreactors with non-Newtonian continuous media." MS thesis. NTNU, (2021).

Galindo-Rosales, F. J., F. J. Rubio-Hernández, and L. Angermann. "Numerical simulation in steady flow of non-Newtonian fluids in pipes with circular cross-section." Numerical Simulations–Examples and Applications in Computational Fluid Dynamics (2010): 3-23.

Guo, Weidong, Gérard Labrosse, and Ranga Narayanan. "The application of the Chebyshev-spectral method in transport phenomena." Springer Science & Business Media, (2013).

Hasanbeigi, Ali. "Energy Efficiency in California's Chemical Industry." Energy (2019).

Hauswirth, Scott C., et al. "Modeling cross model non-Newtonian fluid flow in porous media." Journal of Contaminant Hydrology 235 (2020): 103708.

Howarth, W. J. "Coalescence of drops in a turbulent flow field." Chemical Engineering Science 19.1 (1964): 33-38.

Kufås, Eirik. "Mathematical modeling of coalescence of oil droplets in water flow." MS thesis. Institutt for energi-og prosessteknikk, 2008.

Lee, J. C., and T. D. Hodgson. "Film flow and coalescence-I Basic relations, film shape and criteria for interface mobility." Chemical Engineering Science 23.11 (1968): 1375-1397.

Liao, Yixiang, and Dirk Lucas. "A literature review on mechanisms and models for the coalescence process of fluid particles." Chemical Engineering Science 65.10 (2010): 2851-2864.

Ozan, Suat Canberk, and Hugo Atle Jakobsen. "On the effect of the approach velocity on the coalescence of fluid particles." International Journal of Multiphase Flow 119 (2019a): 223-236.

Ozan, Suat Canberk, and Hugo Atle Jakobsen. "On the role of the surface rheology in film drainage between fluid particles." International Journal of Multiphase Flow 120 (2019b): 103103.

Ozan, Suat Canberk, Jannike Solsvik, and Hugo Atle Jakobsen. "A Bubble Coalescence Kernel Combining the Characteristics of the Film Drainage, Energy, and Critical Velocity Models." Chemical Engineering Science (2023): 118458.

Ozan, Suat Canberk, Hauna Fathmadinda Hosen, and Hugo Atle Jakobsen. "On the prediction of coalescence and rebound of fluid particles: A film drainage study." International Journal of Multiphase Flow 135 (2021): 103521.

Peng, Yan, et al. "Application and prospect of the non-Newtonian fluid in industrial field." Materials Science Forum. Vol. 770. Trans Tech Publications Ltd, (2014).

Rajput, Abhineet Singh, Sarath Chandra Varma, and Aloke Kumar. "Sub-Newtonian coalescence in polymeric fluids." Soft Matter (2023).

Shinnar, Reuel, and James M. Church. "Statistical theories of turbulence in predicting particle size in agitated dispersions." Industrial & Engineering Chemistry 52.3 (1960): 253-256.

Tripathi, A., and R. P. Chhabra. "Drag on spheroidal particles in dilatant fluids." AIChE Journal 41.3 (1995): 728-731.

A MATLAB code

A.1 Non-Newtonian Solver

```
clear all
clc
warning off

global Rp sigma

Rps = [0.0004 0.0005 0.0006 0.0007 0.0008 0.0009 0.001]; %[0.0005 0.001 0.0015
    0.002 0.0025 0.003 0.0035 0.004 0.0045 0.005];

for i=1:length(Rps)
    Rp=Rps(i);

sigma = 0.0728; %[kg/s^2]

% this code with 10-4 won't work for non-newtonian code because there is the
% chance it will run forever
% depending on the outcome, coalescence, steady state or rebound better a
% code that halfs the velocity
% rebound /2
% coalescence /2 and add on top of this value a small value

Vapp0=0.0015;
Vapp0maxStore=Vapp0;
Vapp0max=Vapp0;
Vapp0min=0;
Vapp0minStore=Vapp0min;
reboundswitch = 0;

for y = 1:20 %more iteration for better accuracy
    Vapp0Store(y)=Vapp0;
    outcome(y) = V_critical(Vapp0,0);

    if outcome(y) == 0
        reboundswitch = 1;
        Vapp0max=Vapp0;
        Vapp00=Vapp0/2;
        if Vapp00 < max(Vapp0minStore)
            Vapp00=(Vapp0+max(Vapp0minStore))/2;
        end
    else
        Vapp0min=Vapp0;
        Vapp00=3/2*Vapp0;
        if Vapp00 > min(Vapp0maxStore) && reboundswitch==1
            Vapp00=(Vapp0+min(Vapp0maxStore))/2;
        end
    end

    Vapp0maxStore(y)=Vapp0max;
    Vapp0minStore(y)=Vapp0min;

    if abs(Vapp0 - Vapp00) < 10^(-5)
    Vc = Vapp0max;
    V_critical(Vc,1);
    break
    end

    Vapp0=Vapp00;
```

```
57
58 end
59
60
61 filename = strcat('Vapp0Store_n_115_Rp ', num2str(Rp));
62 filename = strrep(filename, '.', '');
63 save(filename)
64
65 fprintf('Finito, un loop    andato e si volaaa!!\n')
66 % semilogy(min(hStore))
67
68 end
69
70 function outcome = V_critical(Vapp0,saveswitch)
71 global Rp sigma
72
73 %%% data
74 N=200; % then put 300
75 L=0;
76 R=1;
77 dt=0.0001/Vapp0;
78
79 %Astar=10^(-9); %zero to try and then 10^(-2) like before
80 %%%%%!!!!!Canberk: make Hamaker constant a function of Rp
81 Astar=3.731*10^(-20)/(6*pi*sigma*Rp^2)*1000; %first number is the dimensional
      Hamaker constant
82 n=1.15;
83
84 % Discretize r space
85 [D,zc] = cheb(N)
86 [a,b,r] = mapping(L,R,zc);
87 D=a*D;
88 h0min = 0.1;
89 h0=h0min + r.^2;
90 P0=0.00000001*ones(N+1,1);
91 I=eye(N+1);
92
93 %%% Putting them together in a unique unkown vector:
94
95 Pkm1 = P0; Pk = P0;
96 hkm1 = h0; hk = h0;
97 Vapp=Vapp0;
98
99 i = 1;
100 PStore(:,1) = Pk;
101 hStore(:,1) = hk;
102 VappStore(:,1) = Vapp0;
103 tStore(1)=0;
104 t=0;
105 for k=1:1:50000 %longer steps
106     t=t+dt; %keeping track of the time
107     A(1:N+1,1:N+1) = 3/2/dt*I;
108     A(1:N+1,(N+1)+1:2*(N+1)) = n/((1+2*n)*(2^(1/n+1)))*diag(1./r)*D*diag(r)*diag
          ((-D*Pk).^(1/n-1))*diag(hk.^(2*n+1))*(-D);
109     A((N+1)+1:2*(N+1),1:N+1) = 1/2*diag(1./r)*D*diag(r)*D;
110     A((N+1)+1:2*(N+1),(N+1)+1:2*(N+1)) = I;
111
112     rhs(1:N+1,:) = 2*hk/dt-hkm1/2/dt;
113     rhs((N+1)+1:2*(N+1),:) = 2*ones(N+1, 1)+Astar./hk.^3;
114     % Boundary conditions
115     A(1,1:N+1)=D(1,:);
```

```
116     A(1,(N+1)+1:2*(N+1))=zeros(1,N+1);
117
118     A(N+1,1:N+1)= [zeros(1,N) 1];
119     A(N+1,(N+1)+1:2*(N+1))= zeros(1,N+1);
120
121     A((N+1)+1,1:N+1)= zeros(1,N+1);
122     A((N+1)+1,(N+1)+1:2*(N+1))= D(1,:);
123
124     A(2*(N+1),1:N+1)=zeros(1,N+1);
125     A(2*(N+1),(N+1)+1:2*(N+1))=[zeros(1,N) 1];
126
127     rhs(1)=0;
128     rhs(N+1)=(-Vapp+2/dt*hk(end)-1/2/dt*hkm1(N+1))*(2*dt)/3;
129
130     rhs(N+1+1)=0;
131     rhs(end)=0;
132
133     Sol=real(A\rhs);
134     hkp=Sol(1:N+1);
135     Pkp=Sol(N+1+1:2*(N+1));
136
137     if mod(k,10) == 2 %only if number k perfectly divisible by 10
138         k
139         min(hkp)
140         i = i+1;
141         PStore(:,i)=Pkp;
142         hStore(:,i)=hkp;
143         tStore(i)=t;
144         VappStore(:,i)=Vapp;
145     end
146
147 %     if min(hkp) < 0.03
148 %         dt=10^-4;
149 %     end
150
151     if min(hkp) < 0.00001
152         outcome = 1; %'coalescence'
153         break
154     end
155
156     if min(hkp) > 1.1*h0min
157         outcome = 0;
158         break
159     end
160
161     if abs(Vapp)/Vapp0 < 10^-2 && abs(trapz(r,2*pi*r.*Pkp)) < 10^-3
162     % first the V has to be zero but the condition is not enough, also the
163     % film force (Second term) should be small enough
164         outcome=3; %'steady-state'
165         break
166     end
167
168     % higher velocity rebound generally and slow velocities coalescence
169     hkm1=hk; hk=hkp; Pkm1=Pk; Pk=Pkp;
170     Vapp=Force_balance(Pk, r, dt, Vapp);
171     assignin('base','hStore',hStore); %assigns things into the work space
            directly
172     assignin('base','PStore',PStore);
173
174 end
175
```

```
176 if saveswitch == 1
177     filename = strcat('Vapp0 Critical_n_115_Rp_ ', num2str(Rp));
178     filename = strrep(filename, '.', '');
179     save([datestr(now, 'dd-mmm-yyyy-HH-MM-ss') filename])
180 end
181 end
```

A.2 Force Balance

```
1  function Vapp = Force_balance(PStore, r, dt, Vapp)
2  global Rp sigma
3
4  %%%%%!!!!!Canberk:updating the values for air-in-water system. Also
5  %%%%%calculate m instead of guessing it
6  % m = 0.1;
7  rho_c = 1000; %[kg/m^3]
8  rho_d = 1.225;
9  mu_c = 0.001; %[Pa*s] viscosity of continuous phase
10 g=0;
11
12
13 m=4/3*pi*Rp^3*rho_d; %mass of the bubble without the added mass effects
14 Cm = 0.803;
15 m_AD=4/3*pi*Rp^3*(rho_d+Cm*rho_c); %together with the added mass
16 %%%%%!!!!!Canberk: make Oha2 also a function of Rp
17 Oha2 = 8.2*10^(-6); %
18 Oha2 = mu_c^2*Rp^2/sigma/m_AD;
19 %%%%%!!!!!Canberk: In the Re calculation we should use Vapp in dimensional
20 %%%%%form. So Vapp (dimensional)=Vapp(dimensionless)*sigma/mu_c
21 % Re = rho_c*abs(Vapp/2)*(2*Rp)/mu_c;
22 % correct one
23 Re = rho_c*abs(Vapp/2)*(2*Rp)/mu_c^2*sigma;
24 Cd = 24*Re^(-1)*(1+0.15*Re^(0.687)); % Schiller and Naumann (1933)
25
26
27 % ma = m*(1+Cm*rho_c/rho_d);
28 a=m/m_AD*mu_c^2*Rp/sigma^2;
29 b=Cd*Re*pi/4; % drag term coefficient, slows down due to the friction
30 vk1 = -Vapp/2;
31 vk2 = Vapp/2;
32
33 % 2*pi*trapz(r,r.*PStore)*Oha2 --> film force creates huge resistance and
34 % sometimes it is responsible of the rebound effect. Sometimes the Hamaker
35 % Constant can break this resistance and then we can have coalescence, it is
36 % a balance between film force and hamaker whether we have rebound or
37 % coalescence
38 vkp1 = (a*(1-rho_c/rho_d)*g-(-1)*2*pi*trapz(r,r.*PStore)*Oha2-Oha2*b*vk1+vk1/dt)
       /(1/dt);
39 % vkp2 = 0;
40 vkp2 = (a*(1-rho_c/rho_d)*g-2*pi*trapz(r,r.*PStore)*Oha2-Oha2*b*vk2+vk2/dt)/(1/
       dt);
41 %check which particle is -1 in Canberk work (the di in the from of the
42 %intergal)
43 Vapp = vkp2 - vkp1;
44
45 end
```

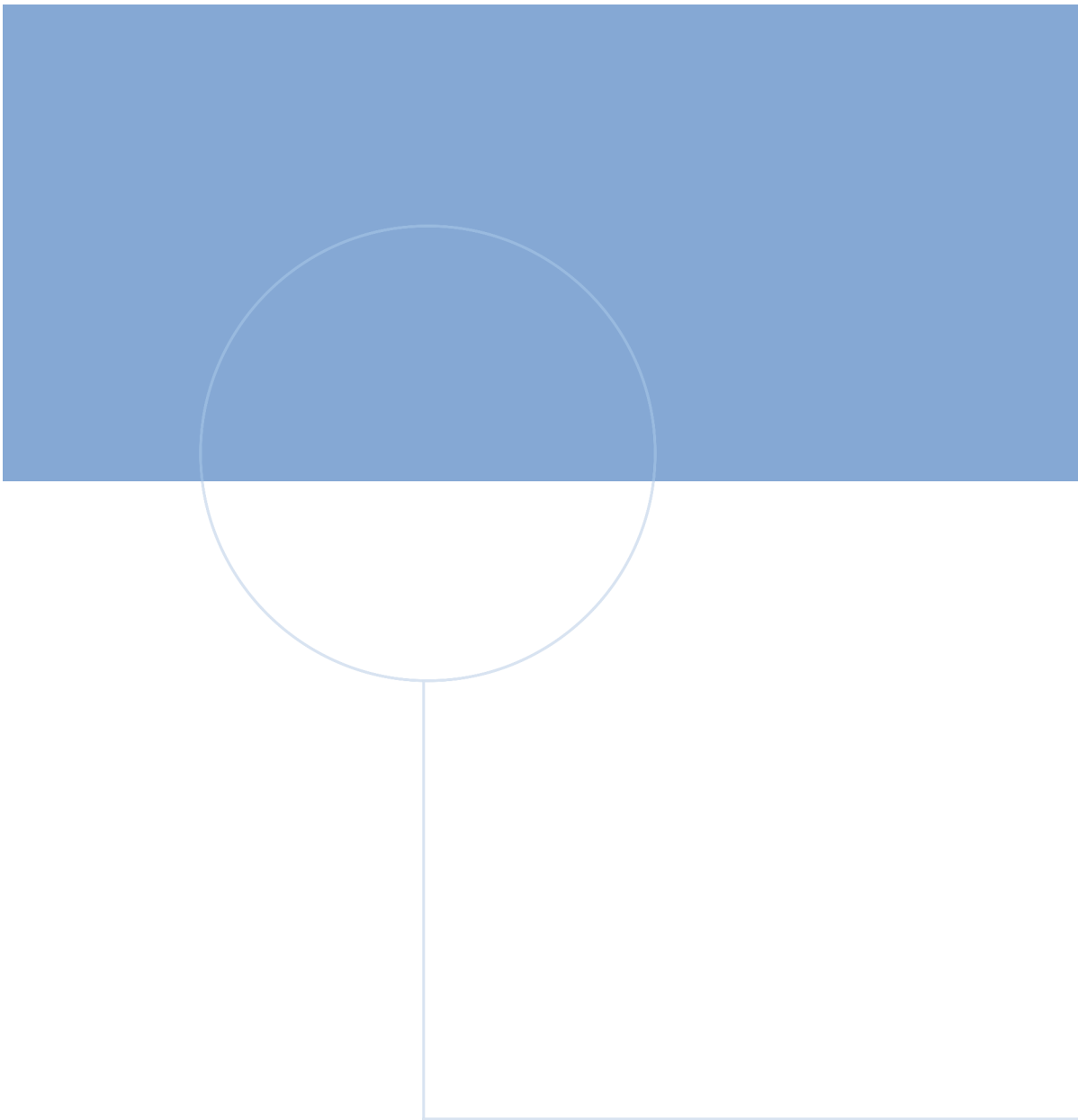

NTNU

Kunnskap for en bedre verden